Test of Fast Neutron Detectors for Spectroscopy with (^{3}He,n) Two Proton Stripping Reactions

by

Elbasher Mohamed Elbasher Ahmed

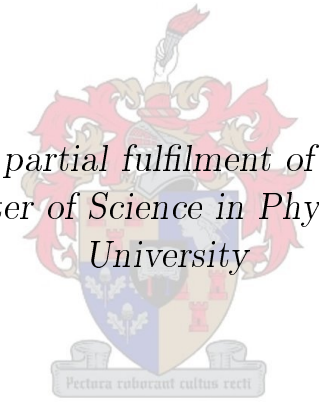

Thesis presented in partial fulfilment of the requirements for the degree of Master of Science in Physics at Stellenbosch University

Faculty of Science - Department of Physics
University of Stellenbosch
Private Bag X1, Matieland 7602, South Africa

Supervisor: Dr. P. Papka
Co-Supervisors: Dr. E. A. Lawrie,
Dr. S. M. Wyngaardt

March 2012

Declaration

By submitting this thesis/dissertation electronically, I declare that the entirety of the work contained therein is my own, original work, that I am the sole author thereof (save to the extent explicitly otherwise stated), that reproduction and publication thereof by Stellenbosch University will not infringe any third party rights and that I have not previously in its entirety or in part submitted it for obtaining any qualification.

March 2012

Abstract

Test of Fast Neutron Detectors for Spectroscopy with (^{3}He,n) Two Proton Stripping Reactions

M. E. A. Elbasher

Faculty of Science - Department of Physics
University of Stellenbosch
Private Bag X1, Matieland 7602, South Africa

Thesis: MSc

March 2012

Nine 100x100x600 mm^3 plastic scintillators, formerly built for the neutron time of flight measurements at iThemba LABS, were refurbished. The position resolution of these detectors was determined using muon cosmic rays and coincident measurement techniques. Average position resolution of $\sim$ 4.28 cm (FWHM) was found. In order to predict the time spectrum of the large-volume detector Monte Carlo simulations have been performed. These simulations aimed at anticipating the separation of statistical neutrons, prompt gamma rays and uncorrelated gamma rays from the fast neutrons emitted in the reaction of interest. One of the neutron detectors was tested using fast neutrons from the ^{232}Th(α,xn) reaction at 42 MeV. Statistical neutrons from fusion evaporation reactions were produced in ^{152}Sm(^{12}C,xn) fusion evaporation reaction. Coincidences between neutrons and gamma rays were successfully identified. Prompt gamma rays and uncorrelated gamma rays were also identified.

Opsomming

Toets van Vinnige Neutron Detektors vir Spektroskopie met (^{3}He,n) Twee Proton Stroopings Reaksies
M. E. A. Elbasher
Fakulteit Wetenskap - Departement Fisika,
Universiteit van Stellenbosch,
Privaatsak X1, Matieland 7602, Suid Afrika.
Tesis: MSc
March 2012

Nege 100x100x600 mm^3 plastiese scintillators, wat aanvanklik gebou was vir neutron vlugtyds meetings by iThemba LABS, was hernu. Die posisie resolusie van die detektore was bepaal deurmiddel van muon kosmiese straling en koïnsidensie meet tegnieke. Posisie resolusie van $\sim$ 4.28 cm (FWHM) was verkry. Monte Carlo simulasies is gebruik om die posisie resolusie van'n groot volume detektor te voorspel. Hierdie simulasies is daarop gemik om onderskeid te maak tussen statistiese neutrone, gelyktydige gamma strale en ongekorreleerde gamma strale vanaf vinnige neutrone in die reaksie van belang uitgestraal word. Een neutron detektor was getoets deur gebruik te maak van vinnige neutrone wat uit die reaksie ^{232}Th(α,xn) by 42 MeV ontstaan. Statistiese neutrone vanaf splitsings verdampingsreaksies, gelyktydige gamma strale en ongekorreleerde gamma strale was geidentifiseer. Statistiese neutrone van samesmelting verdamping reaksies was geproduseer in die reaksie ^{152}Sm(^{12}C,xn). Toeval tussen neutrone en gamma strale was suksesvol geïdentifiseer, gevra gamma strale en ongekorreleerd gamma strale was ook geïdentifiseer.

Acknowledgements

I would like to acknowledge the support of many people who helped me to complete this project. First this study would not have been possible if not for the support and help of my supervisor Dr Paul Papka. I am very grateful to Dr Paul Papka for his unwavering support and for all the indispensable discussions, suggestions and comments. Special thanks go to Dr Elena Lawrie and Dr S. M. Wyngaardt for their readiness to co-supervise my work and for providing me with invaluable guidance and support.

It is my pleasure to thank the academic and administrative staff of Physics Department, Stellenbosch University, for their support and assistance during my study. I would like to thank Mr J. J. van Zyl, Mr David Pool and the Physics Department Workshop for their technical support during manufacturing the neutron detectors.

I gratefully acknowledge the support of the technical staff of iThemba LABS and all members of the Nuclear Physics group and accelerator group. I would also like to extend my thanks to Dr R. Bark for his help regarding the AFRODITE experiments performed in this project.

This work was supported by the African Institute for Mathematical Sciences (AIMS) and the National Research Foundation of South Africa (NRF) via Stellenbosch University and iThemba LABS.

Finally, I would like to thank my family, my parent, my brothers and my sisters for their support, love and encouragement.

M. E. A. Elbasher

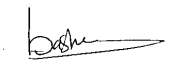

Dedications

To my parent, my mother Um Elhassan Mohey Eldin and my father Mohamed Elbasher, May Allah Subhana Wata'ala reward you. I love You.

Contents

List of Figures

List of Tables

Chapter 1 - Introduction

One of the most important aspects of nuclear physics research is the study of the structure of atomic nuclei. Many theoretical models, such as the shell model, have been developed to predict and describe the nuclear structure in terms of nuclear energy levels. One of the tools widely used to test and investigate nuclear energy levels is the nuclear spectrometers with different nuclear reactions or nuclear radiation sources.
Direct reactions give very specific and selective information on the properties of nuclear levels. This has been exploited extensively with high-resolution magnetic spectrometers when outgoing particles such as, the proton, α and electrons which respond to the electromagnetic field are charged. An example showing a spectrum from the ^{152}Gd(t,p)^{154}Gd reaction is shown in Fig. 1.1. In this spectrum (This spectrum was taken from Ref. [1]), the largest peaks below 2 MeV excitation energy in ^{154}Gd are the 0^+ states. The angular distributions for these states are strongly forward peaked with the maximum of the differential cross-section at 0^o, characteristic of L=0 transitions. This means that the pair of neutrons has been stripped simultaneously off the projectile's nucleus with their spins paired off to angular momentum zero.

Reactions where protons are stripped off the beam nucleus, so that the outgoing particle is a neutron, are difficult to carry out, especially for obtaining sufficient neutron energy resolution. Examples of these neutron- emitting direct reactions are (d,n) and (^{3}He,n), which donate one and two protons to the target nucleus respectively. One-proton stripping can be made with the (^{3}He,d) reaction, but two-proton stripping requires reactions using heavy ions such as (^{16}O,^{14}C) and very good resolutions are still difficult to achieve.

In this study, we wanted to develop and test a fast neutron detector and to use it with time-of-flight techniques. The aim of this project was to use large plastic neutron detectors, with high efficiency for neutron detection, and time-of-flight to separate fast ($\sim$ 27 MeV) neutrons from statistical fusion-evaporation neutrons with energies of less than 6 MeV. The neutrons were to be detected in coincidence with γ-rays detected in the AFRODITE gamma-ray spectrometer with excellent energy resolution [2] (AFRODITE is an acronym derived from AFRican Omnipurpose Detector for Innovative Techniques and Experiments. The AFRODITE located at iThemba LABS which described in section 5.1.1).

1.1 Experimental Challenges of this Project

To carry out this project, the following experimental requirements had to be realised:

• constructing of a detector array as a large-volume-neutron detection system, and

• an appropriate arrangement of the neutron detector to be used with the AFRODITE detector array.

These requirements were met by:

• nine 100X100X600 mm^3 plastic scintillators, formerly built for the neutron time-of-flight measurements at iThemba LABS, were refurbished and are now ready to use, as described in section 3.5.

• two measurements were performed in order to test the time of flight techniques.

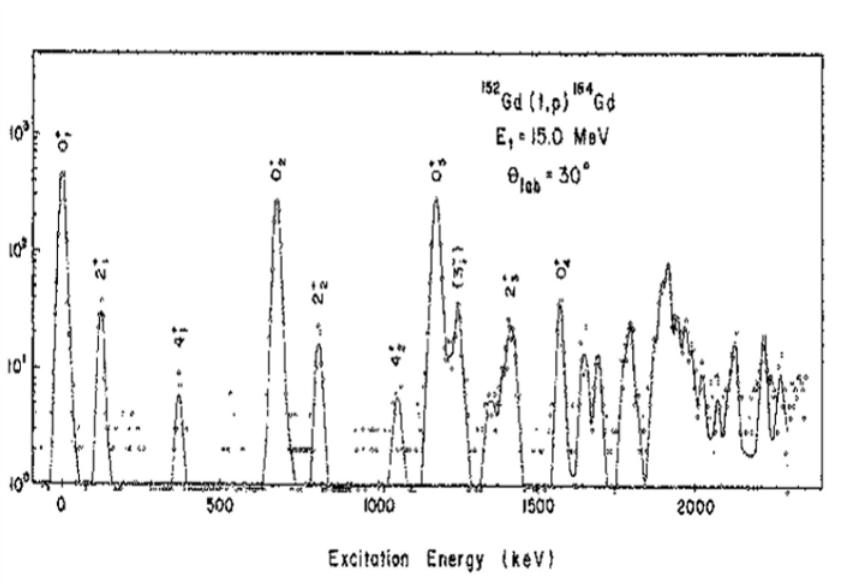

Figure 1.1: A spectrum generated from ^{152}Gd(t,p)^{154}Gd stripping reaction data where two neutrons are transferred to ^{152}Gd and the outgoing particle is a charged particle (proton) [1].

1.2 Fusion Evaporation Reaction and Statistical Neutrons

In nuclear reactions a compound nucleus forms after the collision between projectile and target nucleus. In this case the reaction is called a nuclear fusion evaporation reaction. The compound nucleus is highly excited and has a large amount of energy and angular momentum, therefore it is highly unstable. It cools itself by evaporating statistical particles such as neutrons, protons, deuterons, tritons and α particles. Fig. 1.2 shows an example of this reaction mechanism.

Evaporation residue cross-sections can be determined by direct detection of

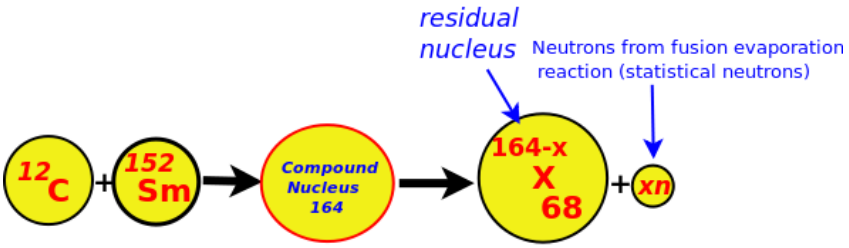

Figure 1.2: Fusion evaporation reactions mechanism.

the evaporation residues themselves or by the detection of the radiation emitted in their de-excitation [3]. It is much easier to identify the evaporation residues with γ-rays.

In this project we have used the following two reactions:

$$^{4}He + ^{232}Th \rightarrow ^{236}U \rightarrow ^{236-x}U + xn, \tag{1.2.1}$$

$$^{12}C + ^{152}Sm \rightarrow ^{164}Er \rightarrow ^{164-x}Er + xn \tag{1.2.2}$$

The (^{4}He,xn) reaction is almost the same as the reaction proposed for the neutron detector test, which is the (^{3}He,n) reaction, since in both of them a light projectile is incident on a heavy target, and statistical and fast neutrons are expected to be produced and detected.

Since it is necessary to acquire coincidence data with the AFRODITE array detectors, the neutron detector was coupled to the AFRODITE data acquisition system. For this coincidence measurement the (^{12}C,xn) reaction was used for more testing, however the target ^{232}Th was the same as the proposed one, and this reaction was available at the time of this project.

1.3 Excited 0^+ States

According to their orbital angular momentum and the spin, there are two kinds of the nuclear state, the positive parity state and the negative parity state. As proposed for this project, the neutrons were to be measured in coincidence with AFRODITE to search for excited 0^+ states in the residual nucleus. The expected residual nucleus was ^{154}Gd. Fig. 1.3 shows some of the excited 0^+ states of this nucleus in different energy bands [4].

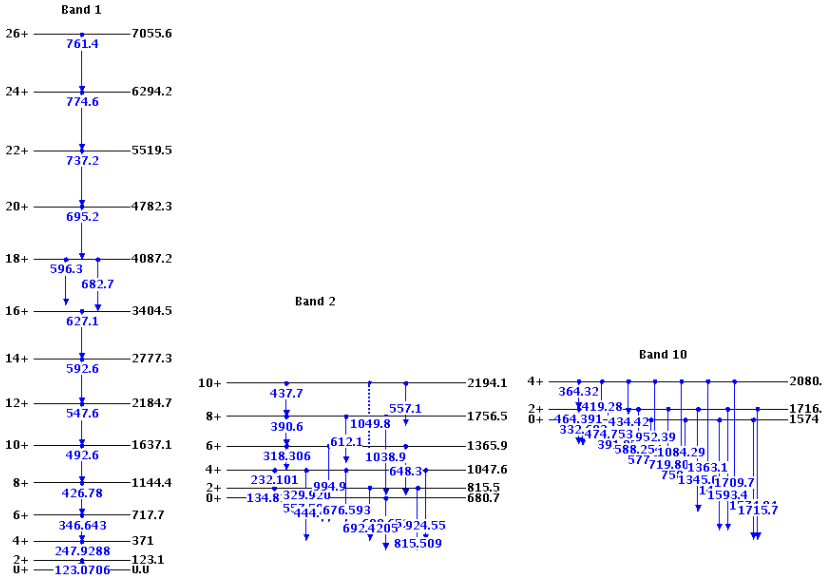

Figure 1.3: Some excited 0^+ states of the ^{154}Gd nucleus in different energy bands [4].

1.4 Nucleon Transfer Reactions

In some heavy-ion induced reactions, energy and angular momentum is transferred, and a result of this dissipation is that a number of nucleons are emitted and transferred between the projectile and the target. An example of this kind of reaction is:

$$ {}^{2}_{1}H + {}^{20}_{10}Ne \Longrightarrow {}^{1}_{1}H + {}^{21}_{10}Ne \tag{1.4.1} $$

In this reaction, 1 nucleon (a neutron) is transferred from the deuterium ion beam to the neon target nucleus.
The number of transferred nucleons in the nucleon transfer reaction could be one (single transfer) or more nucleons (multi-nucleon transfer); the following examples show one-, two- and three-nucleon transfer reactions:

• Single-nucleon transfer reaction:
In this case, as the transferred nucleon could be a single proton or a single neutron, the (d,n) and (d,p) reactions are examples of this reaction, whereby a proton and neutron are transferred from the deuteron beam to the target nucleus respectively.

• Two-nucleon transfer reaction:
(^{3}He,n) and (^{16}O,^{14}C) reactions are examples of two-proton transfer reactions.

1.5 Neutron Detection

It is accepted that neutrons can be classified into three categories depending on their energies:
• Thermal: E $<$ 1 eV
• Epithermal: 1 eV $<$ E $<$ 10 keV
• Fast: $>$ 10 keV
The fast neutrons are expected to originate from the direct reaction. In this study, only fast neutrons with an energy range between 1 MeV and 30 MeV were considered. Neutron spectroscopy plays an important role in experimental nuclear physics. Neutron detection is also used in many applications such as particle physics, material science, cosmic ray detection, reactor instrumentation. The main task of this project was to test a large-volume plastic neutron detector array, and to investigate the ability of these detectors to distinguish neutrons of several tens of MeV from statistical neutrons and gamma rays produced in fusion evaporation reactions.
The process of neutron detection is not straight forward because their neutral nature prevents them from being directly detectable. Since neutrons do not have an electric charge, they do not respond to the electric field and do not ionize atoms. They interact only via direct collision with atomic nuclei, so gaseous ionisation detectors are ineffective. The many challenges posed by neutron detection include the following:

• **γ-ray Background**
One of the main problems in neutron detection is separating the events caused by neutrons themselves and events caused by γ- and x-ray photons. Both of them deposit similar energies after scattering into scintillation detectors. To distinguish between these events, electronic devices such as Pulse Shape Discriminators can be used. The coincidence detection technique can also be used to discriminate between neutron and photon events. One can also apply some conditions such as energy or time gates when the time-of-flight of neutrons is determined. In this project, the detectors were not sensitive to charged parti-

cles as they were placed away from the target behind adequate shielding, see Fig. 5.6.

• **Varying behaviour with energy**
Neutron detectors which use reactions such as ^{6}Li(n,αt) and ^{10}B(n,α ^{7}Li) are very sensitive to low-energy thermal neutrons, and are orders of magnitude less sensitive to high-energy neutrons, since the way neutrons interact with the detector material depends heavily on their incident energies. Scintillation detectors are less sensitive to low-energy neutrons.

The two main methods of neutron detection are neutron capture followed by subsequent secondary radiation and neutron scattering. The methods to detect neutrons can therefore be categorised according to the nuclear processes relied upon, mainly neutron capture or elastic scattering.

1.5.1 Neutron Detection by Elastic Scattering

Elastic scattering is the most common method for detecting fast neutrons. With this method, neutrons elastically scatter off light nuclei, hence transferring a part of their momentum, which results in recoil nuclei. The recoiling nuclei can ionize and excite atoms through collisions. A useful material for fast neutron detection is the hydrogen-containing scintillators such as organic crystals (anthracene, stilbene), liquid scintillators (organic scintillator in an organic solvent), and plastic scintillators (organic scintillator in a polymerised hydrocarbon) [5]. In this project, we used large-volume plastic scintillators (NE102A), to detect fast neutrons.

1.5.2 Detection of Fast Neutrons

A good spectrometer records the energy of an incident particle with high efficiency and resolution. To obtain high efficiency measurements the incident particle must deposit all of its energy within the volume of the detector. This is achieved by using a large-volume detector. In the case of the scintillation spectrometer, the light yield of the material must be known so that the light pulse amplitude can be converted to particle energy. It must be mentioned that there is a non-proportional relationship between the observed light and deposited energy [6]. Measurement of fast neutrons is not straight-forward, since the fast neutrons are not necessarily stopped in the detector, i.e. they leave the scintillator before they have fully deposited their energy. The H/C ratio (number of the hydrogen atoms to carbon atoms) has to be considered before selecting the organic scintillator. More hydrogen atoms increase the neutron interaction rate. N.S. Bowden *et al.* recently demonstrated a hardware technique (detector segmentation) for reducing the effect of the complete

energy deposition; by using detector segmentation one can select the events when the fast neutrons have nearly deposited their total energy [6].

1.6 Time-of-Flight Techniques

The time-of-flight technique is one way of determining the energy of neutrons, since this method measures their flight time along with the flight path. The relativistic or non-relativistic relation between the velocity and kinetic energy makes it possible to obtain the energy spectrum. The neutron time-of-flight method has a long history, with the first reference to such work published in 1935 [7], only three years after the discovery of the neutron. A pair of rotating disks was used to prove, by direct measurement, that many of the slow neutrons are in the thermal velocity range. In this project, the time-of-flight technique was used with plastic scintillation neutron detectors to test the neutron detector as described in section 5.5.1. Simulations of time-of-flight were performed using Monte Carlo methods.

1.7 Outline of the Thesis

In Chapter 2 the neutron properties and neutron detection array are reviewed, followed by a description of the stages of rebuilding the large-volume neutron detectors and the characteristics of the plastic scintillators in Chapter 3. Chapter 4 presents a description of the time-of-flight simulations. Chapter 5 focuses on the equipment, electronics, experimental set-ups and the data acquisition systems used in this project. The data analysis and the results are presented in Chapter 6. Finally, the conclusion and possibilities for future work are discussed in Chapter 7.

Chapter 2 - Neutron Properties, Neutron Detection Array and Particle Accelerators

2.1 Neutron Properties

2.1.1 Introduction

The neutron was discovered by James Chadwick in 1932. It is a subatomic particle with no net electric charge, since it consists of three quarks, two down-quarks (each has a charge of -1/3) and one up-quark (with a charge of +2/3), as illustrated in Fig. 2.1. The mass of the neutron (939.56563(28)MeV/c^2) is

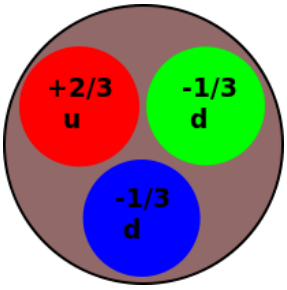

Figure 2.1: Scheme of the neutron with its three quarks, the net electric charge of the three quarks is equal to zero.

slightly larger than the mass of the proton (938.27231(28)MeV/c^2).
Many of the properties of nucleons, such as charge, mass and spin are summarised in Table 2.1, can be explained and deduced from the quantum numbers of their constituent quarks. Chadwick found an appropriate experimental approach. He used the irradiation of beryllium with α-particles from a polonium source, and thereby established the neutron as a fundamental constituent of nuclei. The following equation shows the reaction used by Chadwick:

$$\alpha +^{9} Be \rightarrow \alpha + \alpha + \alpha + n \tag{2.1.1}$$

	u	d	p (uud)	n (udd)
charge z	+2/3	-1/3	1	0
Isospin I	1/2	1/2	1/2	1/2
I_3	+1/2	-1/2	+1/2	-1/2
spin s	1/2	1/2	1/2	1/2

Table 2.1: Charge, mass, isospin and spin of proton and neutron according to their constituent quarks.

Previously, neutral radiation had been observed in similar experiments, but its origin and identity were not understood. Chadwick arranged for this neutral radiation to collide with hydrogen, helium and nitrogen, and measured the recoil energies of these nuclei with the help of an ionization chamber. He deduced from the laws of collision that the mass of the neutral radiation particle was similar to that of the proton and named this particle the neutron [8].

2.1.2 Neutron Scattering

Neutrons scatter elastically and inelastically. In the elastic scattering, the neutron interacts with a nucleus or the magnetic field of unpaired electrons, without exciting any one of them to high excitation energy. The neutron can therefore lose some of its kinetic energy via momentum transfer. In the second type of neutron scattering (inelastic scattering), a part of the energy is dissipated in terms of excitation energy.

Neutron scattering is a useful technique for probing the structure and magnetic order of materials. Since the neutron is electrically neutral, it penetrates deeper through material samples than x-ray photons with a similar wavelength, which interacts with the electron cloud surrounding the nucleus.
Neutrons for scattering experiments can be produced either by nuclear fission in a reactor, (p,n) reactions, ^{7}Li(p,n)^{7}Be for instance, or by spallation when high-energy ($\sim$1 GeV) protons strike a heavy target material (W, Ta, or U). Neutrons for scattering experiments can also be obtained from the ^{252}Cf source, ^{241}Am + ^{9}Be source, etc.

2.1.3 Neutron Tracking

The kinematics of the neutron scattering where a nucleus is impacted by the incident neutron is given by [9]:

$$E_A = \frac{4A}{(1+A)^2} E_n cos^2\theta \tag{2.1.2}$$

where E_A and E_n represent the recoil nucleus and the scattered neutron energies, respectively, A is the mass of the target nucleus and θ is the angle between

the direction of the incident neutron and the direction of the scattered proton. Since the mass of the proton is approximately equal the neutron mass, Eq. 2.1.2 becomes:

$$E_A = E_p = E_n cos^2\theta \tag{2.1.3}$$

If the energy of the incident neutrons E_n is known and fixed, then θ can be determined by measuring the energy of the scattered proton E_p.

2.2 Neutron Detection Array

The aim of this project was to develop a neutron detector array to perform γ-N coincidence measurements with the gamma-ray spectrometer AFRODITE. This type of measurement is performed elsewhere. The following examples show two neutron detection arrays with different specifications, geometries and tasks.
The Modular Neutron Array (MoNA) which is specifically designed for detecting neutrons stemming from breakup reactions of fast fragmentation beams [10].
The Low Energy Neutron Detection Array (LENDA) designed to facilitate the study of (p,n) charge exchange reactions in inverse kinematics using unstable beams was, developed at the National Superconducting Cyclotron Laboratory (NSCL) of Michigan State University .

2.2.1 The Modular Neutron Array (MoNA)

The Modular Neutron Array (MoNA) is a large-area, high efficiency neutron detector that is used in basic research with rare isotopes at the National Superconducting Cyclotron Laboratory (NSCL), the nuclear physics research facility of Michigan State University.
The modular neutron array consists of 144 individual detector modules. Each module is based on a plastic scintillator measuring 10 cm by 10 cm by 200 cm and light guides fitted on each end of each scintillator bar to direct the light into one photo-multiplier tube. Each detector module is wrapped in a light-tight material, allowing the detector array to be arranged in different configurations. In its original configuration, MoNA consisted of 9 vertical layers of 16 detectors stacked closely, having an active area of 2.0 m wide by 1.6 m high. In its current arrangement it is stacked in four separate sections of 2, 2, 2, and 3 layers each, respectively; separated by spaces ranging from 0.5 to 0.8 meters. It measures both the position and time of neutron events with multiple-hit capability. The energy measurement of the neutron is based on time-of-flight measurements. The information that is obtained from the measurements, together with the detected position of the neutron is used to construct the momentum vector of the neutrons [10]. The detection efficiency

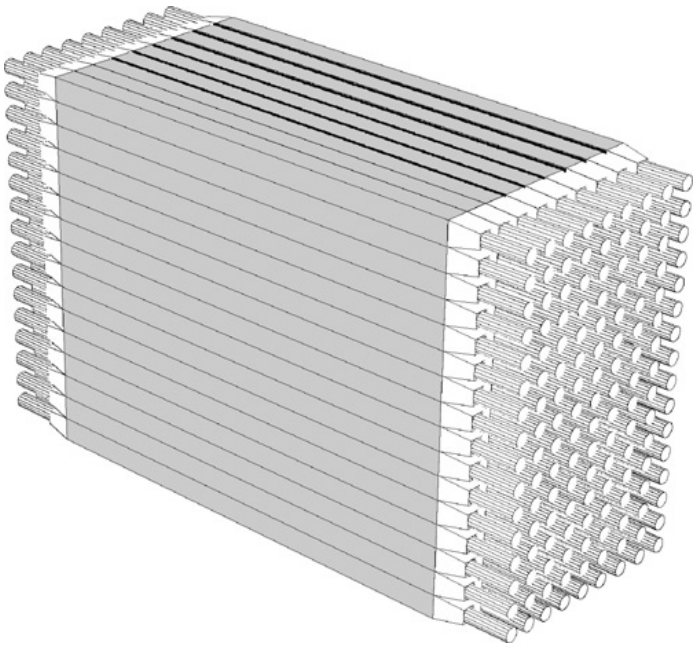

Figure 2.2: A perspective front view of the simulated MoNA detector, showing the plastic scintillator blocks (grey) fitted with light guides and photo-multipliers [10].

of MoNA is maximised for the high-beam velocities that are available at the NSCL's Coupled Cyclotron Facility (CCF). It was designed to have an efficiency of up to 70% for neutrons ranging from 50 to 250 MeV in energy, and expands the possible coincidence experiments with neutrons to measurements which previously were not feasible. The detector is used in combination with the Sweeper magnet [[11], [12]] and its focal plane detectors for charged particles transported between experimental vaults and thus has to be used in combination with the Sweeper magnet installed at the S800 magnet spectrograph [13]. Due to its high-energy detection efficiency, this detector is well suited for experiments with fast fragmentation beams at the proposed ISF (Isotope Science Facility).

2.2.2 The Low Energy Neutron Detection Array (LENDA)

Each module of the array consists of a BC-408 plastic scintillator bar with dimensions of 300x45x25 mm^3 with high-gain photomultipliers attached to each end of the individual modules. For similar detector designs and especially for the detection of low energy neutrons below 400 keV, efficiencies near 70 % have been reported in literature [14]. In each bar, the hit position along its longest side can be determined by combining the time or pulse-height information from each photomultiplier (PMT). The full array will consist of 24 plastic scintillator modules. A prototype module has been developed and tested at

the NSCL. Hamamatsu H6410 PMTs are used to collect and amplify the scintillation light. The PMTs are connected to the scintillator using optical epoxy to ensure optimum transmission of light to the photocathode. The scintillator bar is wrapped with one layer of white filter paper, a layer of aluminium foil and, finally, black insulating tape to ensure proper light propagation through the bar, as well as light-tightness.
The final array has been constructed and characterised in a simple test setup. Results of test measurements and simulations have demonstrated a neutron energy threshold of 130 keV and overall time (position) resolution of $\leq$1 ns ($\sim$4 cm) [15].

2.3 Particle Accelerators

The proposed study of the structure of atomic nuclei and the nature of subatomic particles and their fundamental interactions, required the following equipment [16] with appropriate reactions (to produce the nuclei of interest with sufficient reaction rate):

- accelerator to produce the desired accelerated projectile particle with well-defined energy,
- fixed target,
- beam lines to deliver the beam to the target,
- detectors with high efficiency, and energy resolution/ position resolution.

The particle accelerator is a scientific device using electromagnetic fields to accelerate electrically charged particles to high speeds and to contain them in a so-called ion beam. Ion beams can be produced from any stable isotope from H to U. The latest development includes radioactive isotopes produced during primary collisions, fission or fragmentation. Such ion beams are called RIBs.

2.3.1 Circular Accelerators

In term of shape, particle accelerators can be divided into linear and circular accelerators: In circular accelerators (Cyclotron), particles with charge Q, mass m and velocity v move in a circle with radius r until they reach sufficient energy. Electromagnets with magnetic field B are often used to keep the particle track typically in a circle. The following simple equation shows the

kinematics of this process:

$$QvB = \frac{mv^2}{r} \Rightarrow v = \frac{QBr}{m} \propto Br, \tag{2.3.1}$$

The energy of the particles increase when either the radius of the cyclotron or the magnetic field intensity increased. In this project, as described in section 5.5, we used a cyclotron with a radius of 6.6 m to accelerate α-particles and ^{12}C atomic ions to test the neutron detectors.

2.3.2 The Oscillating Field Accelerators

The oscillating field accelerator, an accelerator that varies only in electric field and does not use any magnetic guide or turning field, is customarily referred to as a linear accelerator or LINAC. In the simplest version of this kind of accelerator, the electrodes that are used to accelerate the particles through attraction/repulsion are connected to a radio-frequency (rf) power supply or oscillator so that alternate electrodes are of opposite polarity.

2.3.3 Beam-Lines, Beam-Dump and Collimator

• Beam-Lines

Ion beams interact strongly with matter, and must be transported under high vacuum medium. The beam-line usually consists of a cylindrical pipe made of metal. In order to obtain a large mean-free path for the beam particle, the beam-line requires a high-vacuum transport medium which allows minimisation of the interaction between the beam particle and air molecules by using vacuum pumps. The beam loss from the collision between the beam particles and the beam-line walls requires the use of dipole and quadrupole magnets and applying an electric field to direct and focus the beam. In order to maintain and monitor the beam, devices such as collimators, water cooling, position monitors and wire scanners, ion pumps, ion gauges and, ion chambers are attached to the beam-line.

• Beam-Dump

The beam-dump is a device usually located at the end of the beam-line to dissipate the energy of the beam of charged particles by absorbing these particles. The absorption of the particles is followed by depositing an amount of heat through the beam-dump. Therefore the material that the beam-dump is made of should meet specific properties, such as a high absorption coefficient and a high melting temperature. A very small number of particles interact with the target material, therefore most of the incoming particles must be

kept away from the detectors (to reduce background emission).

- Collimator

A collimator is a narrow tube used to filter a stream of rays. The collimator permits only the radiation that is travelling in parallel in a certain direction to traverse the entire length. Like the collimator used in this project, collimators often made from Ta.

Chapter 3 - Building and Characterisation of Plastic Scintillation Detectors

3.1 Introduction

There are many types of neutron detectors. Some of these detectors are used only to count the number of neutrons and not measure the energy.
The most common neutron detectors are based on scintillating material. The scintillator (the sensor), consists of a transparent material, usually phosphorus, plastic or organic liquid that fluoresces when struck by neutrons. The most widely applied scintillators include the inorganic alkali halide crystals, of which sodium iodide is the favourite, and organic-based liquids and plastics.
The ideal scintillation material should possess the following properties [17]:

1. It should convert the kinetic energy of charged particles or neutrons into detectable light with a high light output.
2. This conversion should be linear, i.e. the light yield should be proportional to the deposited energy over a wide range of energy.
3. The medium should be transparent to the wavelength of its own emission for good light transport.
4. The decay time of the induced luminescence should be short, so that fast signal pulses can be generated.
5. The material should be of good optical quality and subject to be manufactured in sizes large enough to be of interest as a practical detector.
6. Its index of refraction should be near that of glass (~ 1.5) to permit efficient coupling of the scintillation light to a photomultiplier tube.

3.2 Mechanism

Fast neutrons lose energy when traveling through hydro-carbon scintillator materials by interactions with protons and carbon nuclei. Some of the recoil proton energy is released as scintillation light and the collision kinematics uniquely define the scattering angle of the neutron [18]. The neutrons mainly

interact in the scintillator through the $H(n,n)p$ elastic collision producing recoil protons [19].
When a neutron hits the crystal; a flash of light is produced not because of the direct collision between the neutral particle and a proton in the crystal, but mainly from the energy loss of the proton in the material. The intensity of this light pulse depends on the energy transferred by the neutron to the individual proton in the crystal. The light is transported through the scintillator to the Photomultiplier Tubes (**PMT**s). Some of the photons are then converted into electrons through photoelectric effect by using the PMT equipped with a photocathode. The PMT has several dynodes which multiply the electrons through secondary emission processes. The electrons finally reach the anode, where the accumulation of charge results in a sharp current pulse. Fig. 3.1 shows the detection mechanism related to the plastic scintillator coupled to a PMT.

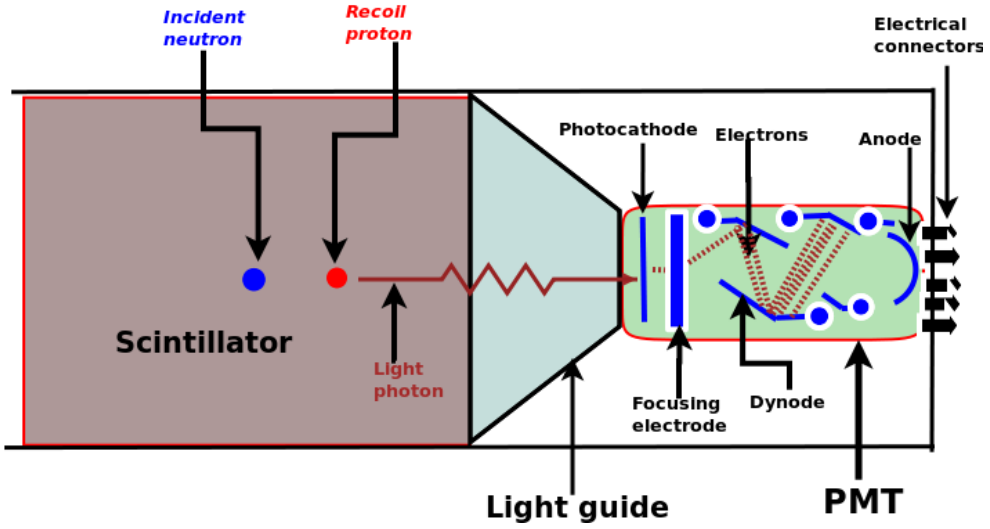

Figure 3.1: Schematic of the mechanism of neutron interaction with the scintillator, conversion of photons into electrons and generation of electrical current pulse.

3.3 Properties of Plastic Scintillators

In order to obtain a good response, many properties of the scintillating plastic should be taken into account. Since the plastic scintillator is an organic material, the atomic ratio, the number of hydrogen atoms to the number of carbon atoms H/C, should be considerable. In the case of neutron detection, the higher the atomic ratio, the more neutrons are scattered, which implies the highest momentum transfer. The second property is the light output which is

how much light is yielded from the incident energy particle, i.e. the fraction of the kinetic energy lost by a particle in a scintillator converted into fluorescent light. It is also very important to consider the time response of the scintillator and pulse shape discrimination. Properties of some plastic scintillators are given in Table 3.1 [17].

Detector	Density (g/cm^3)	Decay constant (ns)	Wave length (nm)	H/C
NE 102	1.032	2.4	423	1.104
NE 105	1.037	$\sim$ 2.4	423	
NE 110	1.032	3.3	434	1.104
NE 111	1.032	1.7	375	1.096
NE 113	1.032	3.3	434	1.108
NE 115		225	385	
NE 140	1.045	$\sim$ 2	425	1.100

Table 3.1: Properties of various plastic scintillators, the melting point and the refractive index of these scintillators are 75° C and 1.58 respectively [17].

3.4 Light Output

3.4.1 Introduction

The differential light output, dL/dx, of a plastic scintillator is a non-linear function of the differential ionization energy loss, dE/dx. The light output for a given energy loss is less when the density of ionization is high. The range-energy curve for $CH_{1.1105}$ (1.1105 is H/C ratio), which is the composition of the plastic scintillator NE102, was determined by interpolating between C,CH and CH_2^5. The Birks and Wright formulae [17] are reasonably good interpretations of the light output of a scintillator detector.

3.4.2 Birks' Formula

The photon production in the scintillator simulated by the Birks formula follows the relation:

$$\frac{dL}{dx} = \frac{S\frac{dE}{dx}}{1 + KB\frac{dE}{dx} + C(\frac{dE}{dx})^2} \tag{3.4.1}$$

where L is the light output, dE/dx is the rate of energy loss of the particle in the scintillator, the KB parameter is an adjustable parameter to fit the

experimental data for a specific scintillator, with the value of S providing the absolute normalisation [17]. This product parameter depends on the type of particle, its energy and on the characteristics of the material itself. The C parameter is only a fitting parameter without any physical significance.

3.4.3 Wright's Formula

Wright suggests:

$$\frac{dL}{dx} = log(1 + a\frac{dE}{dx}). \tag{3.4.2}$$

For energies from 1 to 150 MeV, the rate of energy loss of the particle in the scintillator (dE/dx), can be represented approximately by a power law as shown in Table 3.2: The light output for protons is then obtained by integrating the relation:

Particle	dE/dx
p	$16.94x^{-0.448}$
d	$23.08x^{-0.448}$
t	$27.71x^{-0.448}$
α	$67.76x^{-0.448}$

Table 3.2: The rate of energy loss of the particle (dE/dx) in the NE102 scintillator.

$$L = \int_0^x log(1 + a16.94x^{-0.448})dx \tag{3.4.3}$$

To determine the best value of the parameter a the calculations were compared with the known response of NE102 to protons from 1 MeV to 14 MeV [20]. It was found to be a= 25±2 mg/cm^2/MeV. Fig. 3.2 shows the light output of the p, d, t and α particles, where the energy is in MeV and the range x is in g/cm^2; according to the Wright formula.

3.5 Refurbishing of Plastic Scintillation Detectors

Nine plastic scintillation detectors were rebuilt. These detectors are a part of twelve large-volume plastic scintillation detectors formerly built for the neutron time-of-flight measurements at iThemba LABS. These detectors were used at the NAC in 1990 to study Gammow-Teller strengths in (p, n) reactions at 122 MeV [21]. The optical coupling of these detectors was lost and some of the crystals had become yellow in colour, therefore they had to be refurbished to be able to use them again.

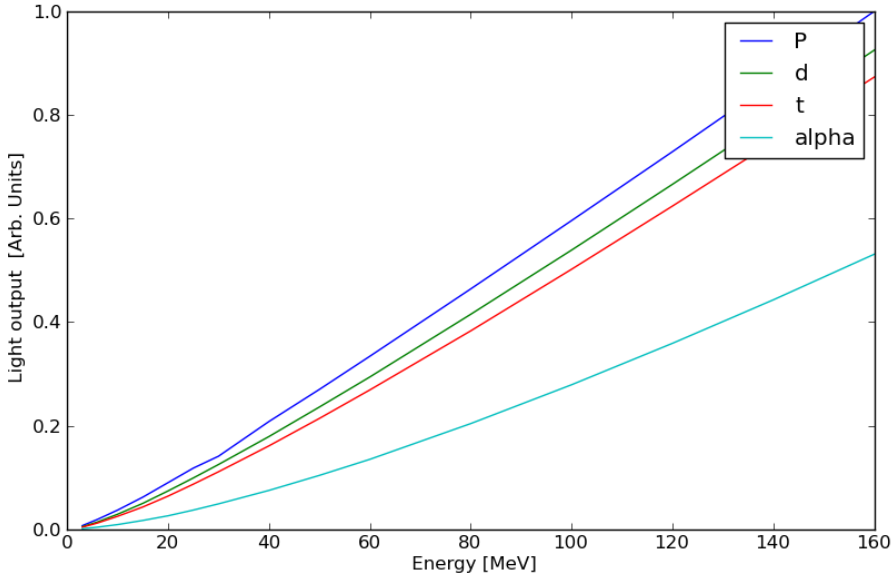

Figure 3.2: The light output of the p, d, t and α particles, where the energy is in MeV according to the Wright formula [20].

Each detector consisted of the following components as shown in Fig. 3.3:
1- A 600x100x100 mm (6000000 mm^3) rectangular bar of NE102A plastic scintillator,
2- Two conical Perspex (PVC) Light Guides (30 cm in length) placed at both ends of the bar.
3- Two Hamamatsu R329 Photomultiplier Tubes (PMTs) with E931 bases.
4- A light-tight aluminium casing.
Some of these components are shown in Fig. 3.4.

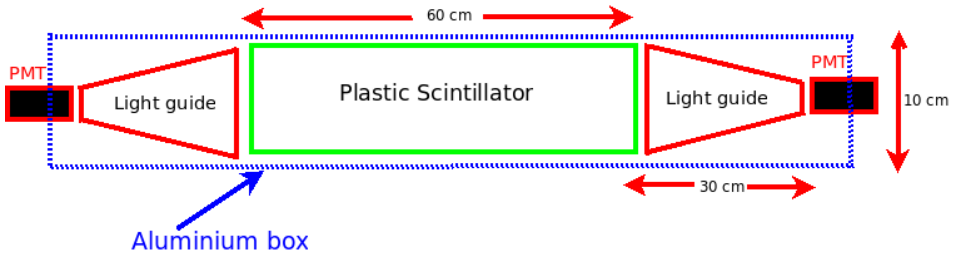

Figure 3.3: Schematic of a large-volume neutron detector.

To connect these components together with optical coupling, a mix of two clear, colourless silicon materials (SIL GEL 612 A and 612 B) of concentration ratio 1:1 was used as gluing material. This silicon has excellent light transmission and high evaporation temperature. It also has an index of refraction of 1.465 which is relatively close to the refractive index of the scintillating plastic NE102A, and has a very flat transmission of approximately 95% for wavelengths between 280 nm and 700 nm.
The minimum time range required to obtain a good coupling between any two of the components (the rectangular bar of NE102A plastic scintillator, the light guides and the PMTs) is about 36 to 48 hours.

Figure 3.4: Some of the components of the neutron detectors, three NE102A crystals coupled to three light guides.

3.5.1 Testing the Photomultiplier Tubes

A ^{137}Cs γ-ray source was used to test the PMTs. A small piece (a cylinder of 3.0 cm in diameter and 2.5 cm in height) of scintillating plastic as a sensor and a small box to protect this scintillating plastic from the ambient light were used after applying a high voltage in the range of -1000 to -1600 Volts to the PMT. A standard spectrometer setup, Preamplifier (PAm) and Multichannel Analyzer (MCA), was used to record and store the response of each PMT. Slight differences in the signals of the PMTs were observed. Some of these PMTs needed more a higher voltage than others to obtain identical signals.

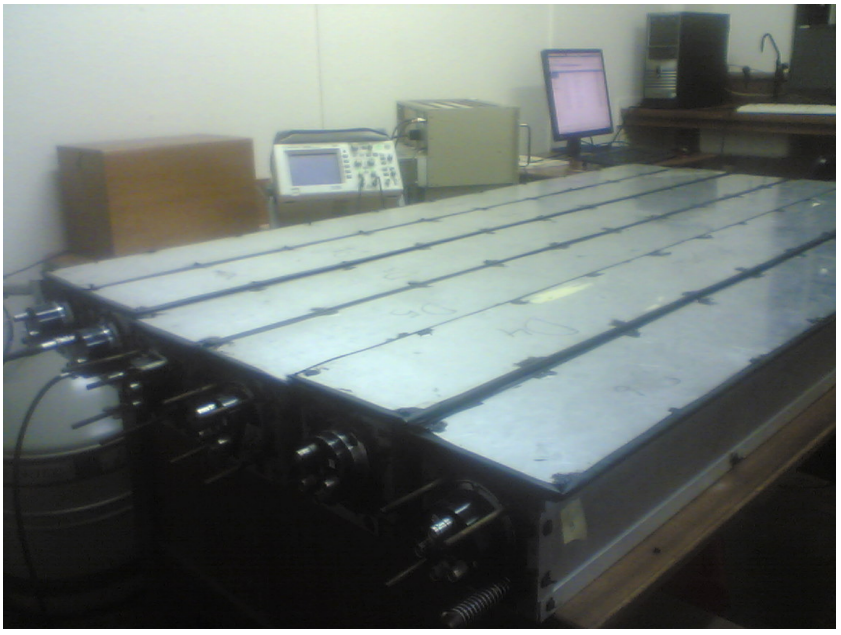

Figure 3.5: The plastic scintillation detectors after rebuild.

3.5.2 Constructing The Plastic Scintillation Detectors

First the detectors were dismantled and each component was cleaned using soft and hard papers. The construction of the detectors was performed following these steps:
1- testing all the PMTs.
2- gluing the components of each detector.
3- improvement of the aluminium boxes by increasing the number of screws to hold the aluminium plates to the structure.
4- putting black paper around each crystal and black silicon inside and outside the whole detector for protection against the ambient light.
5- testing all the detectors by using the spectrometer setup.

It is very important to mention that, a termination resistor of 1MΩ has to be connected to the free anode output of the PMT to obtain a signal from the PMTs. Table 3.3 shows the amplitude and the width of the peaks that are observed on the oscilloscope for different high voltages. Fig. 3.5 shows the neutron detectors after rebuilding.

3.6 Position Measurement

Having two photo-multiplier tubes (PMT) at each end of the crystal gives a degree of position resolution. This is because of the fact that the PMT which is nearest to the interacting point inside the scintillator acquires an amount of

PMT No	High Voltage (-)	Signal Amplitude (V)	Signal Width (sec)	Crystal conditions
PM1	1100	2.4	0.4	Yellow (transparent as well)
PM2	1100	0.5	0.6	Yellow (transparent as well)
PM3	1200	2.2	0.9	Yellow (transparent as well)
PM4	1200	3.0	0.4	Yellow (transparent as well)
PM5	1000	2.2	0.4	transparent
PM6	1000	2.6	0.4	transparent
PM7	1000	4.0	0.2	Yellow (transparent as well)
PM8	1400	1.2	0.2	Yellow (transparent as well)
PM9	1000	4.4	0.2	transparent
PM10	1000	3.8	0.2	transparent
PM11	1300	1.6	0.2	transparent
PM12	1400	1.4	0.4	transparent

Table 3.3: The amplitude and the width of the peaks which are observed on the oscilloscope for different high voltages.

energy larger than the other PMT. The amplitudes of these two PMTs can be related to each other by using an appropriate relation. The position resolution refers to how accurately one is able to determine the position of the interaction point in the detector. Therefore, the information on the position resolution of the system is important and necessary for the analysis of the position spectrum to determine the interaction point of the neutron within the detector [22]. In this project a position coincidence system was set-up to determine the position resolution of the plastic scintillation neutron detector. In this measurement, three detectors (4 PMTs) in coincidence were used, which allowed the selection of a narrow position ($\approx$ 10 cm).

3.6.1 Position Resolution Set-up

To investigate the position resolution of the plastic scintillation detectors one (main) detector and two perpendicular detectors were setup in coincidence, as illustrated in Fig. 3.6 and Fig. 3.7. Four input channels of a digital signal processing Pixie-4 system (XIA LLC [23]) were used to record the energy: two of them were connected to the two PMTs of the detector whose position resolution was to be investigated, and the other two channels were connected to the two PMTs of the other detectors, which were positioned perpendicularly above and below the main detector as shown in Fig. 3.6.
The Pixie-4 system is a multichannel data acquisition system for nuclear physics and other applications requiring coincident radiation detection. It provides digital spectrometry and waveform acquisition for four input signals per module and several modules can be combined into a larger system. Each

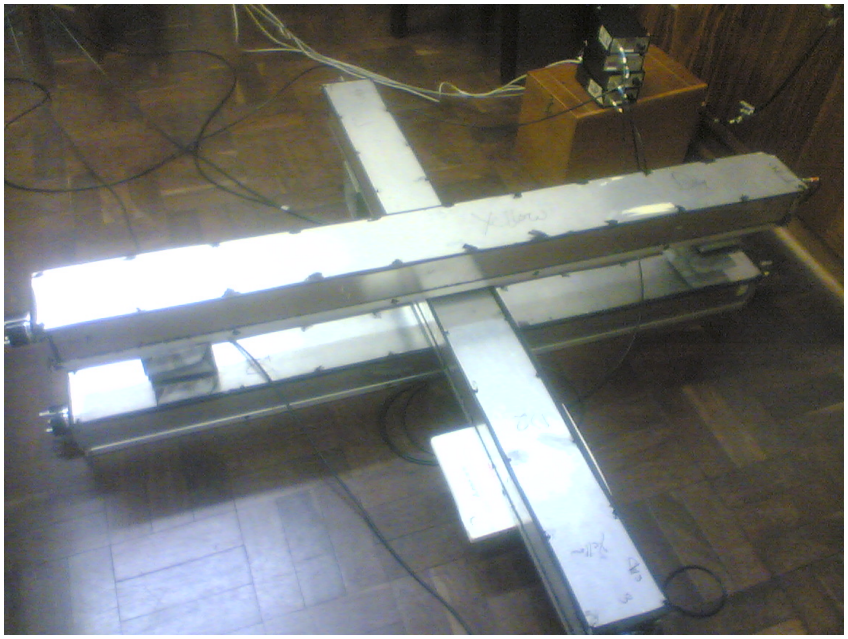

Figure 3.6: The position resolution measurement setup

of the four channels of a Pixie-4 module accepts signals directly from a detector preamplifier or photomultiplier tube. After a digitally controlled gain and offset stage, signals are digitised in a 14-bit ADC at a rate of 75MHz.
Muon cosmic rays were used as a source of radiation. Muons are unstable elementary particles similar to the electron (having a negative electric charge and a spin of 1/2) with a mass of 105.7 MeV/c^2, which is about 200 times the mass of the electron. Muons can be produced by the collision of cosmic radiation with atoms high (10 km) in the atmosphere. Muons have a lifetime of 2.2 μs as measured in a reference frame at rest with respect to the muon [24].
In this set-up the scintillator (i.e. the crystal) of the main detector was divided into six parts, each 10 cm in length. The energy distribution of the muons was measured at each position. The fact that the muons were incident in a straight line and that the three detectors (with 4 PMTs) were in coincidence, ensured that the muon cosmic rays were detected at a specific position whose range through the detector was 10 cm (see Fig. 3.7). The experiment was repeated six times by changing the position of the main detector. Table 3.4 shows the position resolution of each position and the average. To obtain these values, we used the convolution theorem. The convolution theorem was used to optimise the square distribution of each position into Gaussian distribution by shifting the origin of the square distribution function to the position of the peak of the Gaussian distribution function. Then, from the standard deviation σ of the Gaussian distribution, the position resolution (FWHM) was calculated from

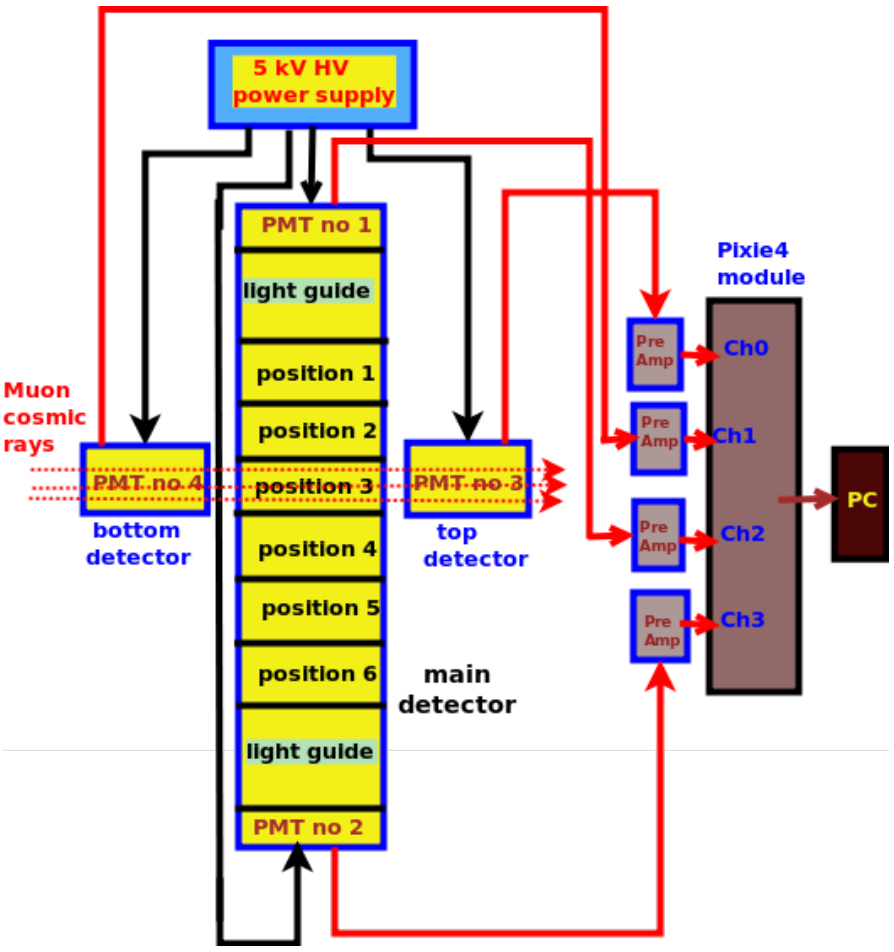

Figure 3.7: The block diagram of the electronics and the set-up used in the position resolution measurements.

the data as:

$$FWHM = 2\sqrt{2\ln 2}\sigma = 2.35\sigma, \tag{3.6.1}$$

where FWHM is the full Width at half maximum.

Position	Position Resolution (FWHM)
0-10 cm	4.30 cm
10-20 cm	3.87 cm
20-30 cm	4.90 cm
30-40 cm	4.50 cm
40-50 cm	4.10 cm
5-60 cm	4.02 cm
Average	4.28 cm

Table 3.4: The position resolution of each position and the average.

3.6.2 Position Sensitivity

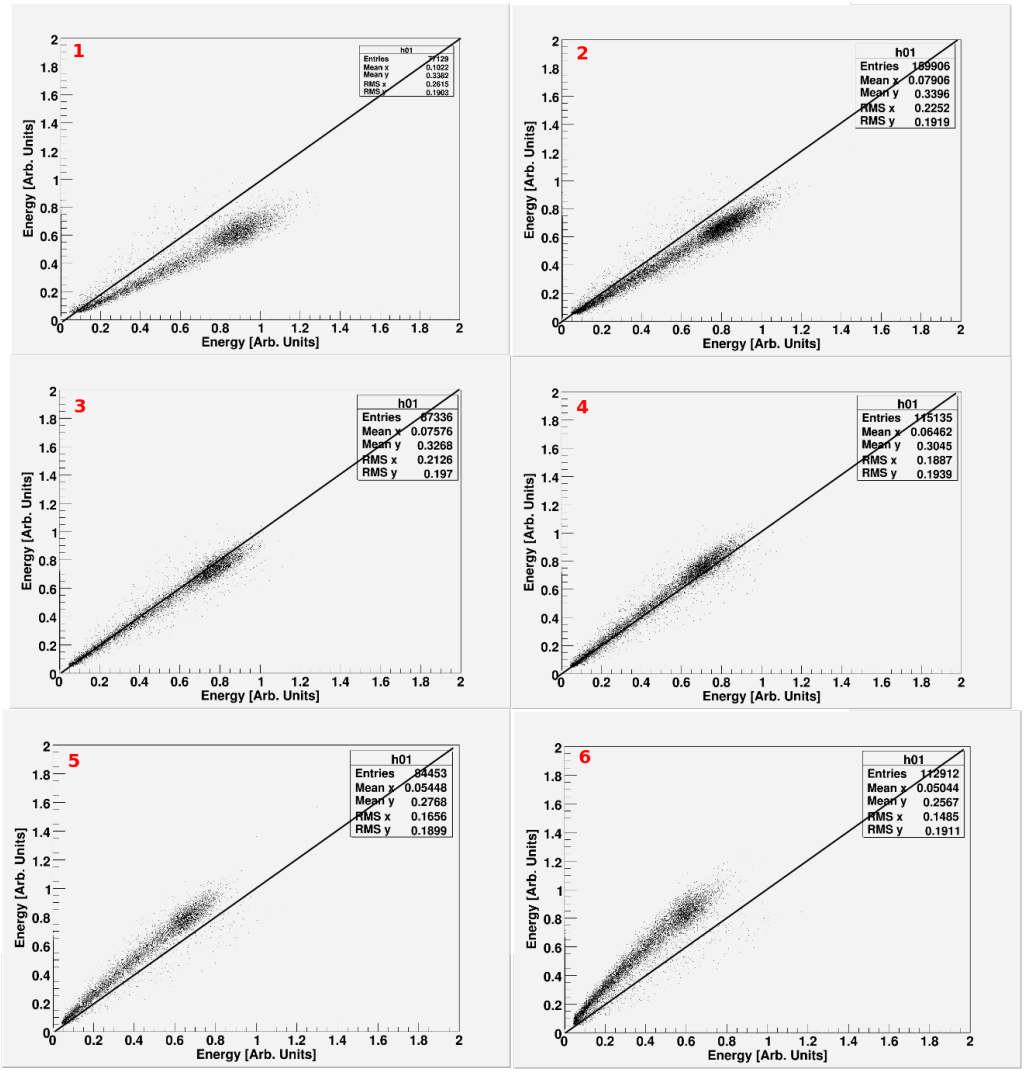

Figure 3.8: The PM tube near the interaction point receives a larger amount of photons than the PM tube on the other side.

Muon cosmic rays were used to test the response of the neutron detector. As described in section 3.6, a specific set-up was established to study the position resolution of the neutron detector. The plastic scintillator of the neutron detector was divided into six sections and, a data file was recorded for each section. The data analysis yielded proof that the distribution of the energy between the two PMTs at both ends of the detector was sensitive to small shifts in position, i.e. the energy distribution was sensitive to small changes in the position of the detector. Fig. 3.8 shows the position sensitivity for the six positions. The PM tube near the interaction point receives a larger

amount of photons than the PM tube on the other side. This effect is observed in spectra 1 to 6 (position 1 to 6), where the signal is gradually decreasing on PM 1 while increasing on PM 2. At position 3 and 4, the interaction point is located in the middle of the scintillator bar and consequently the signals are approximately equivalent on both PM tubes

3.6.3 Gain Matching

The muon energy spectrum (E_1 and E_2) measured from the PMTs of the main neutron detector did not match. To match the gain of these two spectra, the energy spectrum of the second PMT (E_2) was multiplied by the gain factor G which was 1.66. This value was obtained from the polynomial fitting. Fig. 3.9 shows those two spectra after matching the gain at position 3 where the light is guided to the PM tubes throught an equivalent amount of transparent material. The muon energy peak was expected at about 20 MeV

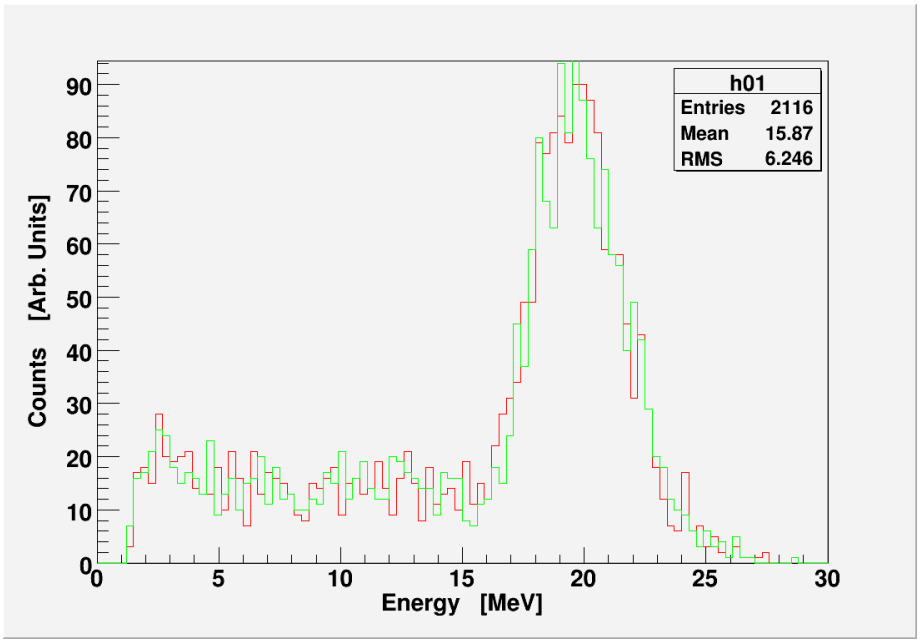

Figure 3.9: Muon energy spectra of the two PMTs of the main detector at position 3, after gain matching.

Since the neutron detector had two PMTs at each end (Fig. 3.3), the following formula could be used to obtain the position spectrum (P):

$$P = \frac{E_1 - E_2}{E_1 + E_2}, \tag{3.6.2}$$

where: E_1, E_2 represents the energy deposited in each PMT assuming linear decay of the signal with the distance between the interaction point and PM tube.
Then to obtain the right position of each spectrum which corresponds to each part (position 0-10 cm) of the plastic scintillator, some parameters were added as:

$$P = a + b\{\frac{(E_1 - E_2)}{(E_1 + E_2)}\}, \tag{3.6.3}$$

As the position P varies from 0 to 600 mm, the ratio $\frac{(E_1-E_2)}{(E_1+E_2)}$ takes a minimum value of -0.5 at $P = 0$ mm and maximum value of 0.5 at $P = 600$ mm. Therefore the values of the parameters a and b are 300 and 600 respectively.
Eq. 3.6.3 used under the following conditions to gate on the muon peak:
$(0.8 < E_3 < 1.2)$, $(0.8 < E_4 < 1.2)$,
where: E_3 and E_4 (in Arb. Units) represents the energies deposited in the PMT of the top and bottom detectors respectively (Fig. 3.6 and Fig. 3.7.) These two separate detectors (E3 and E4) were used only, to ensure that the muon cosmic rays were detected at the required position.
Fig. 3.10 shows the position spectrum of each position obtained with Eq. 3.6.3.

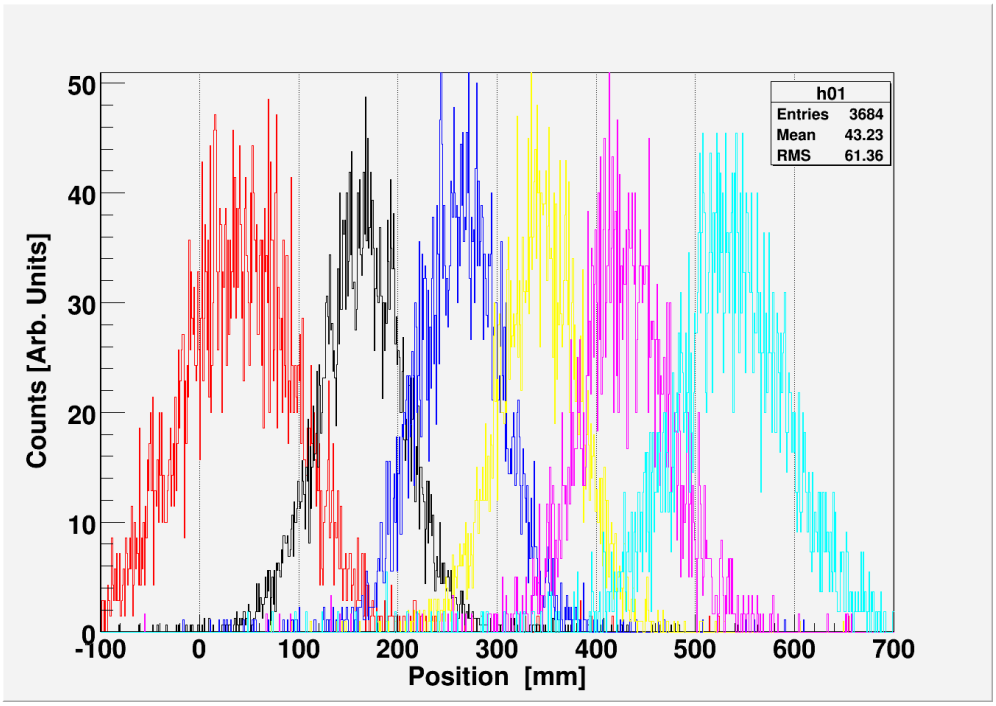

Figure 3.10: Position spectra for six positions of along the main detector. The 10-cm intervals are portrayed with dotted lines.

Chapter 4 - Time-of-Flight Simulations

4.1 Introduction

Monte Carlo simulations were performed to predict the time spectrum to be measured with the large volume detector. These simulations were aimed at anticipating the separation of statistical neutrons, prompt γ-rays and uncorrelated γ-rays from the fast neutrons emitted in the reactions of interest. Fig. 4.1 shows the geometry of the experimental set-up. The position of the collimator and the beam dump are presented, since they are expected to be a source of γ-rays and of some neutrons besides the target.

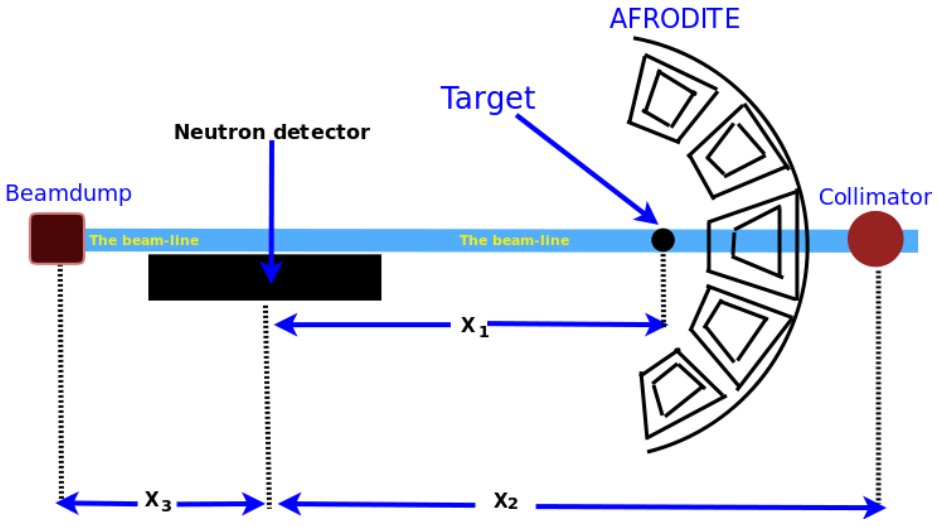

Figure 4.1: The position of the target, collimator and the beam dump from the neutron detector, all of which lay along the beam line.

To determine the time of flight the following non-relativistic equation can be used:

$$E = \frac{1}{2}mv^2 \tag{4.1.1}$$

where E, m and v represent the kinetic energy, the mass and the speed of the neutron respectively.

Since $(v = d/t)$, Eq. 4.1.1 becomes:

$$E = \frac{1}{2}m\frac{d^2}{t^2} \Longrightarrow t = d\sqrt{\frac{m}{2E}} \tag{4.1.2}$$

where d and t are the flight distance and time respectively.
If we take the value of the energy E in MeV, d in meters, the time of flight in nano second is given by:

$$t = \frac{72.25d}{\sqrt{E}}\text{ns}, \tag{4.1.3}$$

The error in the energy (ΔE) can be calculated by differentiating Eq. 4.1.3 as:

$$\Delta E = 0.027\frac{\Delta t}{d}E^{3/2} \tag{4.1.4}$$

The distance d between the neutron detectors and the target as in the proposed experiment of this project, is 1.5m. Therefore the time that the neutron needs to travel this distance is:

$$t = \frac{108.34}{\sqrt{E}}\text{ns}, \tag{4.1.5}$$

The expected energies of the fast and statistical neutrons are 28.3 MeV (from direct reactions, see Eq. 4.1.3) and 6 MeV (maximum energy from fusion evaporation reactions) respectively. According to Eq. 4.1.5, the flight time of these neutrons are, 20.37 nano-seconds and 44.24 nano-seconds respectively, whereas γ-rays take 5 nano-seconds to travel 1.5 m. Therefore the fast neutrons, statistical neutrons and γ-rays can be separated well by using the time-of-flight technique.
In the simulations a number of parameters have been considered, such as the flight distance inside the detector, the exact interaction point, neutron energy distributions, the solid angle covered by the detector, the cross sections for p(n,n) elastic scattering with the detector material, time shift and wraparound, detector geometry and effective thickness. These parameters were taken into account within the Python code as presented in Appendix A.

4.2 Time-Shift and Wrap-around

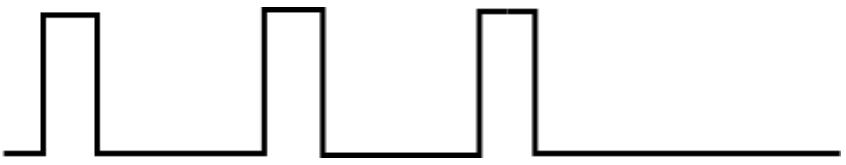

Figure 4.2: The time interval between any two bunches of the beam.

As the beam particles are produced from a circular accelerator (Cyclotron) with the use of the radio-frequency (RF) technique, the beam particles come in bunches (packets). The time interval between any two bunches represents the time necessary for one bunch to make half an orbit in the cyclotron. Fig. 4.2 is a representation of the discriminator signal derived from the RF signal. The time shift occure when such an event happens after such a particular time period, which is given by:

$$Time_{Shift} = RF_{n+1} - RF_n \tag{4.2.1}$$

To obtain the right value of the time of flight (T_{tof}) the time-shift must be added to the original time of flight (T_{real}) (the time taken by the particles to travel from the source to the detector), as.

$$T_{tof} = Time_{Shift} + T_{real} \tag{4.2.2}$$

In some cases, the value of the time interval between two bunches is less than the time-of-flight. For example, when the stop pulse arrives after the RF signal, the next pulse will stop the TAC (Time to Amplitude Converter). The measured time-of-flight is then found to be less.

4.3 Q-value and Neutron Energy

The following reactions were expected to be used in the proposed experiment (see Appendix B) with 22.5 MeV ^{3}He ion beam:

$$^3He +^{152} Sm \rightarrow n +^{154} Gd, \tag{4.3.1}$$

therefore the corresponding Q_v can be given as:

$$Q_v = 14.93 - 74.76 - 8.071 + 73.7 = 5.8 \text{ MeV} \tag{4.3.2}$$

Using the assumption that the residual nucleus ^{154}Gd is at rest and in its ground state, the neutron energy (E_n) can be calculated from the laboratory energy E_{lab} and Q_v as:

$$E_n \approx Q_v + E_{lab} = 5.8 + 22.5 = 28.3 \text{ MeV} \tag{4.3.3}$$

In this project we used the following reaction to test the neutron detector with a 42 MeV α-particle beam:

$$^4He +^{232} Th \rightarrow^{236-x} U + xn \tag{4.3.4}$$

Following the same steps, the Q_v of 2 proton pick up reaction is:

$$Q_v = 2.424 + 35.45 - (2 \times 8.071) - 38.148 = -16.416\text{MeV}, \tag{4.3.5}$$

and the neutron energy is:

$$E_n \approx \frac{E_{beam} + Q_v}{2} = \frac{42.0 - 16.416}{2} = 12.792\text{MeV}. \tag{4.3.6}$$

^{235}U was also expected in this experiment as:

$$^4He + ^{232}Th \rightarrow 1n + ^{235}U, \tag{4.3.7}$$

with Q_v in ^3He pick-up reaction:

$$Q_v = 2.424 + 35.45 - 8.071 - 40.920 = -11.117\text{MeV}, \tag{4.3.8}$$

then the energy of the only one neutron produced in the reaction is:

$$E_n \approx E_{beam} + Q_v = 42.0 - 11.117 = 30.883\text{MeV}. \tag{4.3.9}$$

Most of the events, however, were expected to undergo nuclear fission, with the production of fast direct neutrons with energy E_n expected to be $\sim$ 10 MeV.

4.4 Simulations of the Time of Flight

To calculate the time-of-flight, the following quantities are required:
• the kinetic energy of the incident particles, which allows the calculation of the velocity of these particles.
• the source-detector distance, i.e. the distance between the detector and the source of particles such as the target, the collimator and beam dump.
• the distance travelled by the particles inside the detector, which depends on the mean free path of the particles in the detector material (NE 102A plastic scintillator).
• calculating the mean free path requires knowledge of the cross-section of elastic scattering and the number of particles per unit of volume of the detector material.

Table 4.1 is a representation of a neutron incident in the plastic scintillator. The fast neutrons are expected to follow a Gaussian distribution with an energy peak around 10 MeV (Eq. 4.3.6). Fast neutrons are also expected to be produced in the fission of the ^{236}U compound nucleus which is the dominant reaction. The counts of the slow neutron are expected to decrease exponentially with an energy range of 0 to 6.0 MeV. Some γ-rays from different sources are randomly generated. The proposed target-detector distance (d) is 150 cm, from the assumption that the detector is placed along the beam line, so the maximum vertical target-detector distance would be 5 cm, which represents the half width and half height of the detector. Therefore the real target-detector distance (r_1) varies from 150 cm up to the maximum value of 150.2 cm (negligible difference) which is given by the equation:

$$r_1 = \frac{d}{\cos\theta\cos\Phi} \tag{4.4.1}$$

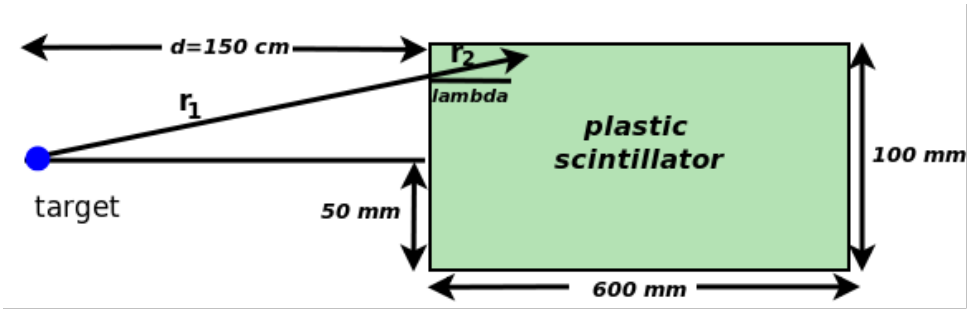

Figure 4.3: Geometry of the detector.

The particles	Statistical Neutrons	Fast Neutrons	Gamma-rays
Expected Energy	0-5 MeV	peak around 10 MeV	< 2 MeV
Expected Distribution	Exponential	Gaussian	Uniform

Table 4.1: Particles used in the simulations with their energies.

where θ and Φ vary from 0 up to $\arctan(5/d)$. Following the same argument, the distance traveled by the particles inside the detector r_2 (see Fig. 4.3) is given by:

$$r_2 = \frac{\lambda}{\cos\theta \cos\Phi} \tag{4.4.2}$$

where λ represents the mean free path which is always less than the length of the scintillator (< 600mm).
λ is calculated from the following relation:

$$\lambda(E) = \frac{1}{\sigma(E)N} \tag{4.4.3}$$

where σ(E) is the cross-section for elastic scattering at incident neutron energy E and N is the number of particles per unit of volume, which is given by:

$$N = \frac{\rho}{A} N_a \tag{4.4.4}$$

where ρ is the density of NE 102A which is 1.032 g/cm^3, A is the molecular weight (202), and N_a represents the Avogadro number (6.02×10^{23}). Therefore the number of particles per unit of volume is:

$$N = \frac{1.032 \times 6.02 \times 10^{23}}{202} = 3.076 \times 10^{21} \tag{4.4.5}$$

and the number of hydrogen atoms (N_H) is given by:

$$N_H = N \times r = 3.076 \times 10^{21} \times 0.52 = 1.599 \times 10^{21}, \tag{4.4.6}$$

where r is the fraction of the hydrogen atoms in NE 102A. The Marion and Young formula which is an empirical fit to the hydrogen scattering cross-section was used for the cross section. According to Marion and Young, the cross-section (in barn) is given by:

$$\sigma(E) = \frac{4.83}{\sqrt{E}} - 0.578 \tag{4.4.7}$$

4.5 The Main Steps of the Simulations

1. Calculate the cross-sections.
2. Generate the neutron energy.
3. Test if the particle enters the detector.
4. Test if the particle exits from the detector's walls.
5. Calculate the effective thickness.
6. Determine the interaction point.
7. Generate the neutron position.
8. Generate some gammas from the different sources.
9. Calculate the time of flight.
10. Define some limits for the displays.
For more detail, the Python code is presented in Appendix A of this thesis.

4.6 Results

For the (α,xn) reaction test experiment 5000 events were randomly generated to obtain a time spectrum with beam energy of 42 MeV. The typical values of time-shift and wraparound used in this simulation were 90 and 500 ns. The distances (x_1, x_2 and x_3) between the different sources of γ-ray (the target, collimator and the beam dump) and the neutron detector (Fig. 4.1) were 1.28, 3.45 and 0.58 m respectively. The maximum time for the displays was 200 ns and the maximum energy was 30 MeV. We used only one neutron detector, therefore the dimensions of the NE 102A scintillator were kept constant at 100, 100 and 600 mm for the length, width and height respectively.
Fig. 4.4 shows the calculated time-of-flight; the fast neutrons appear in this spectrum at 137 ns to 147 ns and 155 ns to 300 ns and the statistical neutron in the range of 400 ns to 500 ns. The γ-ray from the collimator, the target and the beam dump appear at 97 ns, 127 and 337 ns respectively. Fig. 4.5 shows the predicted spectrum of the Time versus the Position matrix; this spectrum is very useful for distinguishing between fast and statistical neutrons and γ-rays. The discrimination between fast and statistical neutrons and γ-rays is made possible owing to the shape of the straight vertical lines appearing in this spectrum. The two straight lines with slight tilt correspond to the fast neutrons whereas the three other lines correspond to γ-rays. As illustrated in

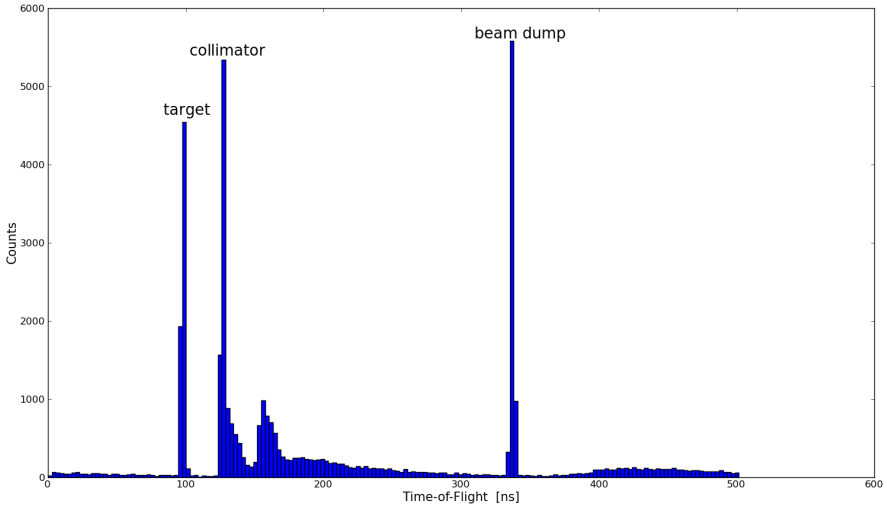

Figure 4.4: The time-of-flight spectrum.

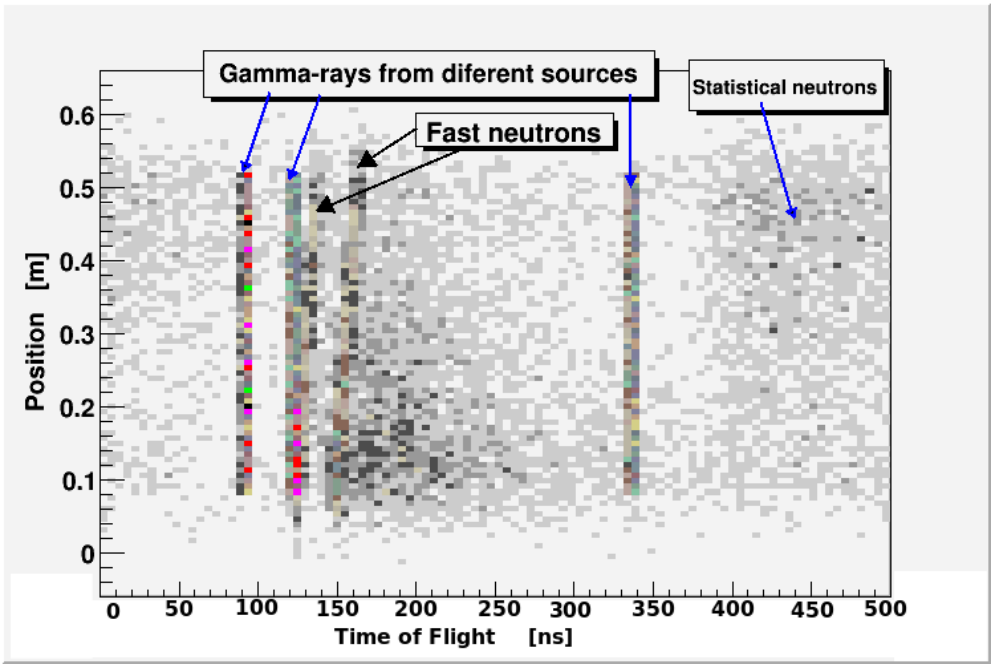

Figure 4.5: Position vs time-of-flight matrix. This position is within the detector.

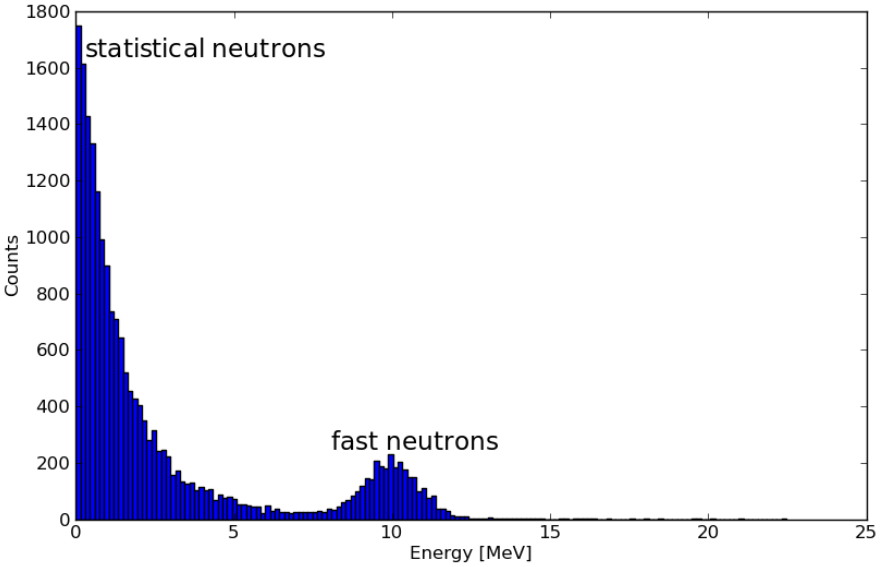

Figure 4.6: Simulated neutron energy spectrum.

Fig. 4.6, the fast neutrons have a Gaussian distribution with an energy peak at 10 MeV and the statistical neutrons follow an exponential distribution with maximum energy less than 6 MeV. From the comparison of the numerical results with experimental data, a good agreement between the simulated spectra and the measurements was shown in this project as described in Chapter 6. The simulation predicts a noticeable contribution to the time-of-flight spectra from the γ-rays coming from the target, the collimator and the beam dump.

Chapter 5 - Experimental Set-up and Electronics

5.1 Introduction

The facilities of iThemba LABS were used to test the neutron detectors. The ion beam was produced by the SSC/SPC2 accelerators and the coincidence measurement test was performed with the AFRODITE γ-ray spectrometer. These facilities also include the detection and the electronic (Digital and Analog) systems.

5.1.1 iThemba LABS Facility

iThemba Laboratory for Accelerator Based Science (LABS) has two solid-pole injector cyclotrons as shown in Fig. 5.1. These are the K= 8 (SPC1) used to accelerate light-ions and the K= 10 (SPC2) for heavy-ion and polarised hydrogen ion beams. The K= 200 separated-sector cyclotron (SSC) (dimensions: 13.2 m in diameter and 7 m in height) has four sector magnets. In this project the required ^{4}He and ^{12}C ion beams with energies of 61 and 64 MeV respectively were delivered by using the SPC2 in conjunction with the SSC. These beams were steered from the SSC along the X, P_1 and R beam-lines (see Fig. 5.1) and finally through the F-line to the AFRODITE γ-ray spectrometer (discussed in section 5.1.2).

5.1.2 AFRODITE Array

AFRODITE, is an acronym derived from AFRican Ominpurpose Detector for Innovative Techniques and Experiments [2]. AFRODITE is an array comprised of nine Compton suppressed clover detectors (High purity Germanium (HPGe)) and eight four-fold segmented LEPS detectors (Low-Energy Photon Spectrometers). The array consists of 18 square and 8 triangular facets. The two square facets at 0° and 180° with respect to the beam direction accommodate the beam pipe. The top most square facet (of the AFRODITE) at 90° with respect to the beam direction supports the pneumatic target positioner. The other 15 square facets are used for mounting the detectors as shown in Fig. 5.2. In order to improve the peak-to-total ratio, a Compton-suppression

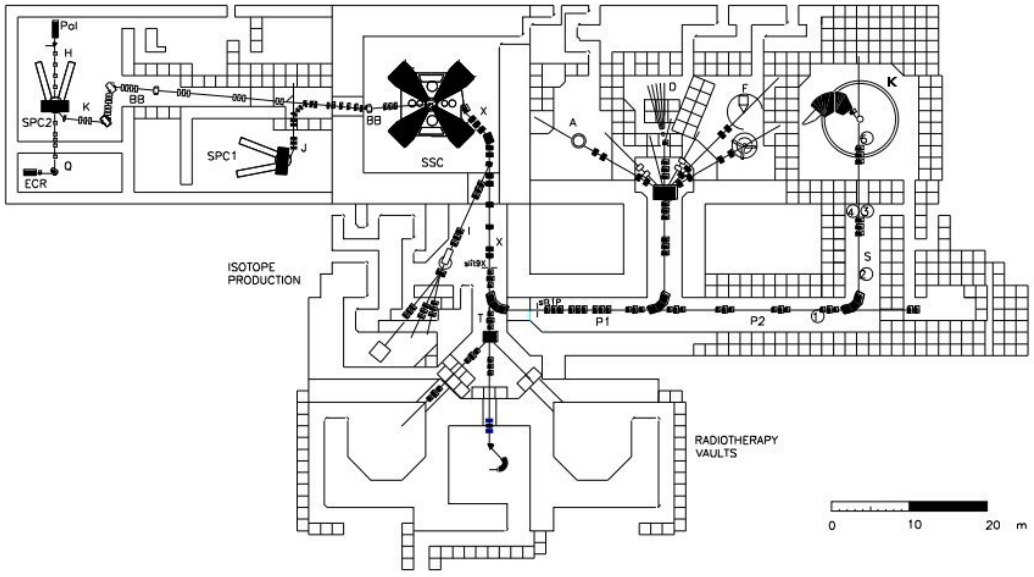

Figure 5.1: Plan-view of the iThemba LABS facility (see Table 5.1).

shield which is made of bismuth germanate $Bi_4Ge_3O_{12}$ (BGO) is used to cover the clover detectors [25].

We used the AFRODITE array in conjunction with a neutron detector, as shown in Fig. 5.5.

5.2 Electronics

Data acquisition systems (DAQ) are required for obtaining digital values from detection devices. The digital values are more easy to process than analog waveforms, which are the output of most of the detectors.

5.2.1 Analog Electronics

Signals from the detectors are usually analog signals with their amplitude reflecting the amount of energy deposited. Analog signals have an advantage in that they can represent any fractional quantity, by outputting an equivalent fractional quantity of voltage or current.
Analog electronics need some shaping with spectroscopy amplifiers to feed to the ADC. They also require fast amplifiers to generate some logic for triggering.

Abberviation	Name
A	Scattering chamber beam-line
D	Collimated neutron beam facility
ECR	Electrons Cyclotron Resonance ion source (at the basement)
F	High-energy γ-ray detectors (AFRODITE)
IP	Isotope production facility
L	Low-energy experimental vault
P	Polarized-ion source (basement)
SPC1	Solid-pole injector cyclotron for light-ions
SPC2	Solid-pole injector cyclotron heavy and polarized ions
SSC	Separated-sector cyclotron
TC	Isocentric neutron therapy
TR	Horizontal proton therapy
TL	Isocentric proton therapy (under development)
K	k600 magnet spectrometer

Table 5.1: Abbreviations used on the plan-view in Fig. 5.1

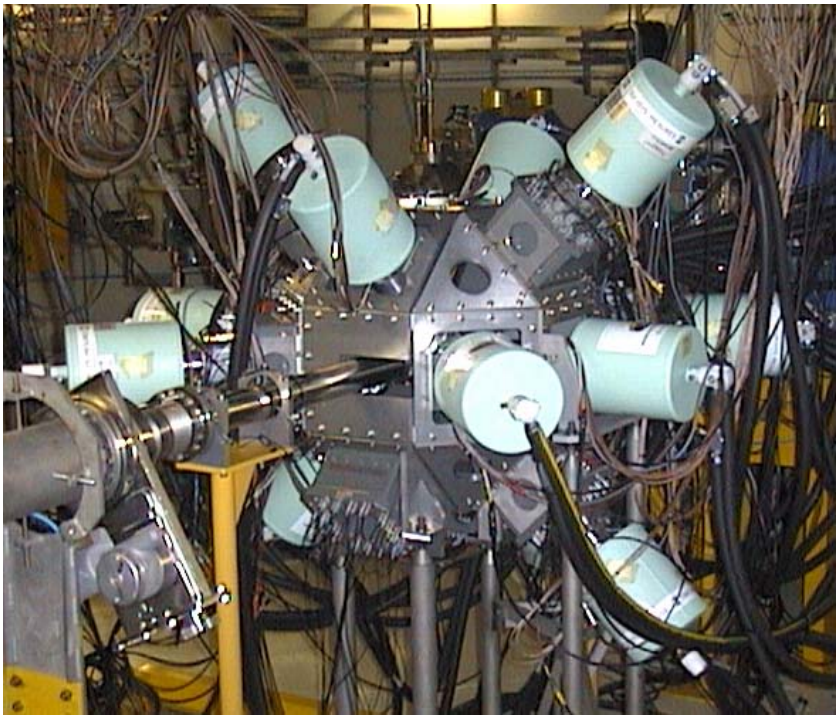

Figure 5.2: The right and the left (the array is closed on the picture) caps of the AFRODITE aluminium frame. The frame supports the LEPS and Clover (housed inside the BGO shield) detectors.

5.2.2 Digital Signal

Digital signals are different from analog signals in that [26] there are generally only two levels of voltage: high and low. These different voltage levels are arranged in a sequence to describe the value being transmitted. For convenience, regardless of the actual voltage levels used, a "high" is called a 1, and a "low" is called a 0. Each signal level must be transmitted for at least a certain period of time called the Bit Time. A single signal level for a single bit time is called a Bit. From bits, we have Binary Numbers, a collection of bits that can be arranged to form larger quantities than the simple numbers 0 and 1.
While there are many ways of implementing an ADC, three conceptual steps are followed [26]:
•the signal is sampled.
•the sampled signal is quantised.
•the quantised signal is digitally coded.
Fast digitisation and sampling of a pulse require an algorithm to work out the amplitude and time signal. Data are stored in different ways; only amplitude and time (2 bytes for E, 3 bytes for time) or pulses are stored (up to 5 μs at 75 MHz).
In this project we used the ADCs several times as a part of the electronics and the data acquisition systems. With the MIDAS DAQ system, the ADCs code only the amplitude (2 bytes/pulse), while with Pixie4, the ADCs were used to sample at 75 MHz (2bytes/13 ns).

Analog to Digital Converter

The Analog-to-Digital Converter (ADC) is an electronic system (device) which converts the analog input signal into a digital output signal and this process takes place through a mathematical function. Digital information can be manipulated and read by computers [26].
The quality of the digitisation is measured in bits which define the step size between two increments. Gamma-ray spectroscopy require 13- to 14 -bit digitisation, while a standard oscilloscope uses only 7-bit ADCs (128 increments)

Timing Filter Amplifier

A Timing Filter Amplifier (TFA) is a device used to enhance timing analysis by shaping pulses and to permit optimising the signal-to-noise ratio for timing measurements. In this project we used this device to shape the pulses coming from the neutron detector before they were furnished to the discriminator (see Fig. 5.4). As the neutron detectors are fitted with PMTs with huge gains, it was convenient to use the TFA because of its rapid rise time, high output drive, and relatively high gain capabilities.

Pulse Shape Discriminator

The pulse shape discriminator is used to distinguish between events caused by neutrons and γ-rays in such a detector. Pulse shape discrimination (PSD) in organic scintillators has been known for many years particularly PSDs with liquid scintillators (NE213/BC501A).
The difference between neutron and γ pulses can be seen by comparing the pulse decay time. The decay time for neutrons is longer than for γ-rays [27]. Neutrons induced more long lived molecular states in organic scintillators than γ-rays, but the scintillators used in this project did not allow that.

Constant Fraction Discriminator CFD

There are many techniques that can be used to obtain and pick out timing information, such as [28]:
•the leading edge discriminator which is a very common method, but with a penalty of time walk.
•the clipping stub technique. This method requires the use of a cable delay, so it is difficult to achieve stability and high density integration.
•the constant fraction technique which is of great interest has been used for many years because of its negligible time walk.
CFDs are designed to [29] produce accurate timing information from analog signals of varying heights, but with constant rise time. They do this by splitting the input signal, attenuating half of it and delaying the other half, then feeding the two output signals (two halves) of 1V with the width and delay adjustable into a fast comparator with the delayed input inverted.

Time-to-Pulse-Height Converter

Time-to-pulse-height converter TPHC is a device used to measure the time interval between two events. Using this device enables transforming the time difference (between start and stop) into amplitudes [30]. Usually the start pulse is initiated after a useful delay and the stop pulses are standardised in a discriminator.
In this project, a TPHC was used to measure the time-of-flight of neutrons and γ-rays from the ^{232}Th (α,xn) reaction detected in the neutron detector. The start pulse was the output pulse of the discriminator from the neutron detector, and the stop information originated from the beam radio-frequency signal (RF), as illustrated in Fig. 5.4.

Tail Pulse Generator

A tail pulse generator (TPG) is a device used for simulating the outputs signal of the detectors and the related electronics. A TPG can be used to simulate the shorter pulses of plastic scintillators. These devices, for example, offer good linearity and stability. In this project, we used the TPG to generate a short rise time and long decay time signal with an amplitude proportional to the amplitude of the square signal coming from the Time-to-Pulse-Height Converter, as shown in Fig. 5.4. This trick was used to get the XIA system to record the time as it does not understand square-shaped signals.

Time-to-Digital Converter

A Time-to-Digital Converter (TDC) is a device mainly used in signal processing and electronic instrumentation to convert signals of time pulses into digital signals. Therefore the output of the TDC is the time of arrival of each input pulse. For that reason TDCs are connected to a discriminator in many applications. Knowing the time of arrival of each pulse allows the measurement of the time interval between a start and a stop pulse.
In this project, TDCs were used with the ^{152}Sm(^{12}C,xn) reaction to test the neutron detector by measuring the relative time of neutrons and γ-rays. In these measurements the relevant time difference was between the pulse coming from a HPGe clover detector of the AFRODITE array and the pulse coming from the neutron detector.

5.3 Data Analysis

5.3.1 SimSort

SimSort [31] is a low-energy nuclear physics data analysis program, which proposes a general approach of data analysis for γ-ray, neutron and charged particle spectroscopy. SimSort is also a simulation code which is able to generate data using identical configurations for both simulation and analysis purposes. In this project we used SimSort to reduce the experimental data. SimSort can be used for Doppler corrections, kinematic reconstruction and other general tasks required for nuclear physics measurements. The results of a SimSort analysis are written in ROOT tree format. Fig. 5.3 shows the schematics of the SimSort code.

5.3.2 ROOT

The main tool used for the analysis was ROOT, an object oriented data analysis framework initiated at CERN by René Brun and Fons Rademakers [32]. It contains a large number of packages concerning different parts of data analysis,

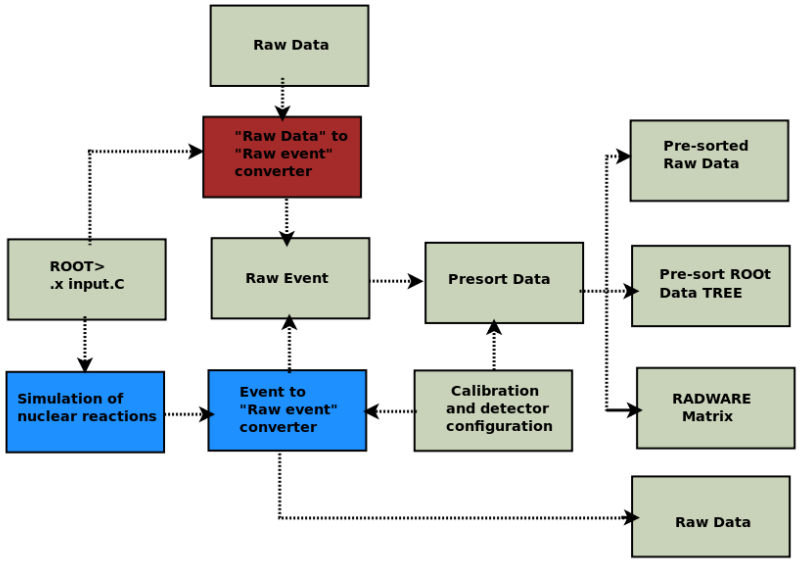

Figure 5.3: A flowchart of SimSort code [31].

for example histogramming handling, curve fitting, minimisation and statistics tools.
The framework of ROOT is closely bound to a C^{++} interpreter called CINT. This means that one actually uses C^{++} as a scripting language for rapid prototype development of programs. Then the same code can be compiled to take advantage of the fast running of an executable machine language [33].

5.4 Data Acquisition Systems

The main components of a data acquisition system are:
• Signal conditioning circuitry to convert sensor signals into a form that can be converted to digital values. Examples of conditioners are amplifiers or filters.
• Analog-to-digital converters (ADC), which convert conditioned sensor signals to digital values.
• Event builder; to get the information from the ADC and pack it into an event.
• A central unit to collect the events and store them on a hard drive.
In addition to the DAQ hardware components, DAQ software is needed in order to connect the DAQ hardware with a PC.
In this project, two different DAQs were used; the Pixie4, which is a compact electronic device with 4 input channels, containing an ADC card; and the VME of the AFRODITE. The VME crate hosts the computer that communicates with the TDCs, and ADCs and build the events later stored on magnetic tape or hard drive

Dead Time and Triggering

The dead time is the time during which the system is busy coding and transferring data. This time must be subtracted to obtain the live time. When a combination of analog and digital electronics is used in the detection system, the dead time introduced by these electronics is the time between the two successive recorded events. The largest contribution of dead time comes from the DAQ system when it is busy coding and transferring the data. Dead time is introduced from analog electronics concerns the shaping time of a spectroscopy amplifier. The storage of the event and digitisation process during conversion of the analog signal to the digital signal causes dead time.
In some cases there is no need to record all the events that occur during the experiment. A trigger system is used to decide which events must be kept (potentially interesting events) and which events should be eliminated from the coding and storage. In this project, in order to identify the events that should be recorded for later analysis, we used a trigger system, called the $\gamma - \gamma - n$ (gamma-gamma-neutron) trigger, during the ^{152}Sm(^{12}C,xn) reaction test experiment (see section 5.5.2) which enabled the selection of only one event coming from the HPGe clover detectors and one event from the plastic neutron detector. We chose this particular trigger to identify the correlation between neutrons and gamma rays with a reasonable count rate. As the detection efficiency of the gamma-ray spectrometer and the neutron detector is lower than the γ-γ-n rate, sufficient count rate for efficient identification of γ-n correlation would not expected.

5.5 Experimental Set-up

All the experiments and measurements presented in this thesis are described and discussed in this section. Two main sets of measurements were performed in this project. These experimental set-ups were used for the time-of-flight and relative time measurements. These set-ups differed with regard to the data acquisition systems that were used, which enabled the use of different triggers for specific events of interest. In the time-of-flight measurement, the coincidence between the neutron detector and the RF was used, and in the relative time measurement, the coincidence was set between the neutron detector and the HPGe clover detector from the AFODITE.

5.5.1 The ^{232}Th(α, xn) Reaction Test

To distinguish between the statistical neutrons from the ^{232}Th(α,xn) fusion evaporation reactions, fast neutrons and γ-rays, the time-of-flight was measured using one NE102 plastic scintillation neutron detector. A 42 MeV α particle ion beam and ^{232}Th as target nucleus with a thickness of $\sim$ 120 μg/cm^2 was used. Fig. 5.4 shows the block diagram of the electronics and the setup

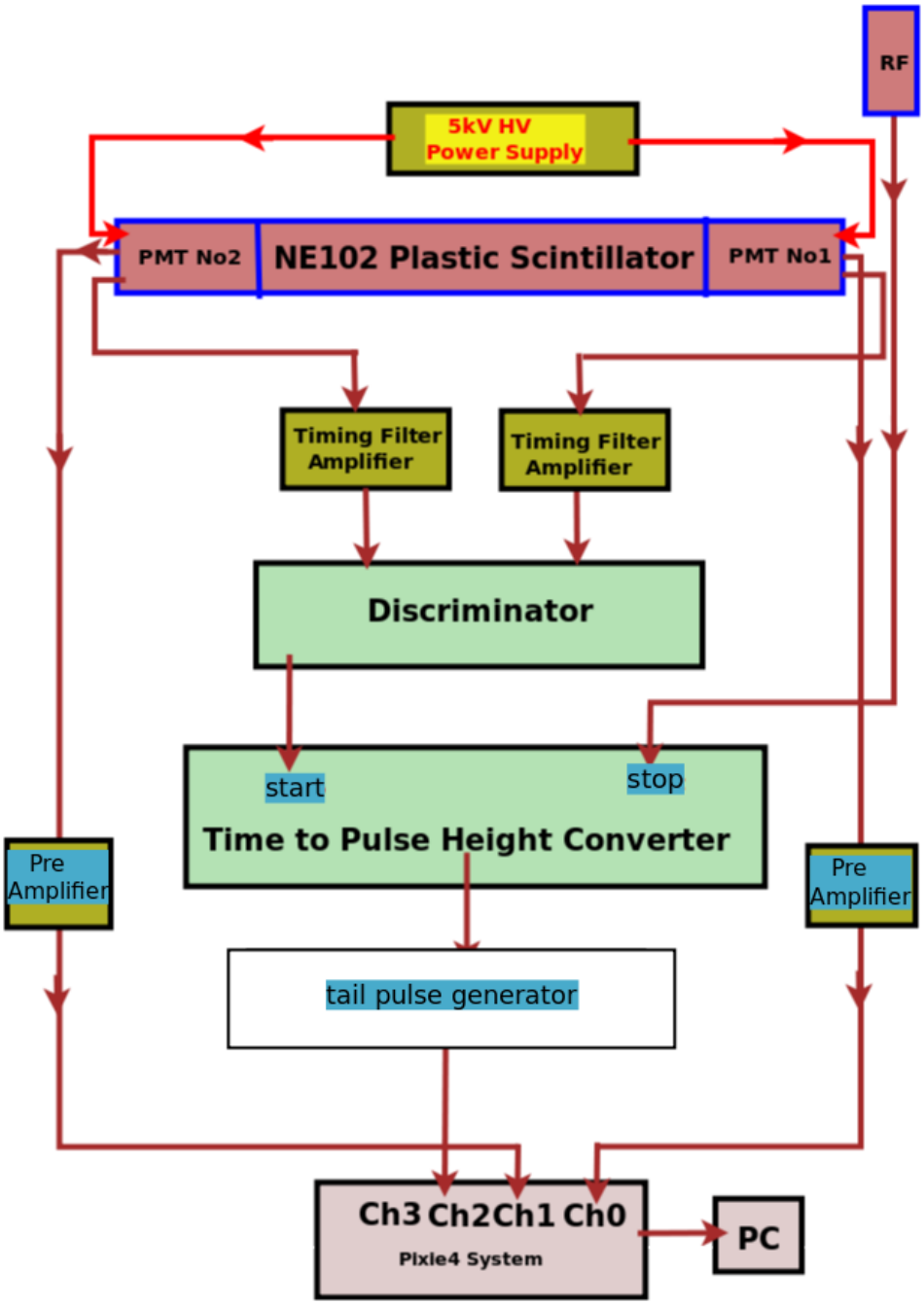

Figure 5.4: Schematic diagram of the electronics and the set-up used in the ^{232}Th(α,xn) reaction test.

used in these measurements.
In order to obtain the energy spectrum, the energy pulse signals from each PMT of the NE102 plastic scintillation neutron detector were amplified through a preamplifier, then these signals were acquired through the Pixie4 module. The time signal from the second PMT was amplified by using a Timing Filter

Amplifier. Then a discriminator was used to differentiate between the amplified signals. A Time-to-Pulse-Height Converter was used to convert the time difference of the two input time signals. The first input (START) was the output of the Discriminator and the second one (STOP) was the time signal which came directly from the beam pulse signal as a time reference after passing through a Time Delay. Before the time signal entered the Pixie4 module, which does not work at all with the square signal coming from the Time-to-Pulse-Height Converter, the signal was shaped with a Tail Pulse Generator.

5.5.2 The ^{152}Sm(^{12}C,xn) Reaction Test

As another test for the neutron detector, a relative time measurement experiment was performed using the same neutron detector. The neutron detector was set in coincidence mode with the AFRODITE γ-ray spectrometer, as shown in Fig. 5.5. Data were acquired under the condition of a neutron-γ trigger, by setting the neutron detector in coincidence with the Clover detectors. We used the reaction ^{152}Sm(^{12}C,xn) with a 64 MeV ^{12}C ion beam delivered by the Separated-Sector Cyclotron (SSC) at iThemba LABS. The target was ^{152}Sm with a thickness of $\sim$ 5 mg/cm^2. The experiment was performed over two weekends. TDCs were used to measure the relative time between the Clovers, and the NE102 plastic scintillation detector.

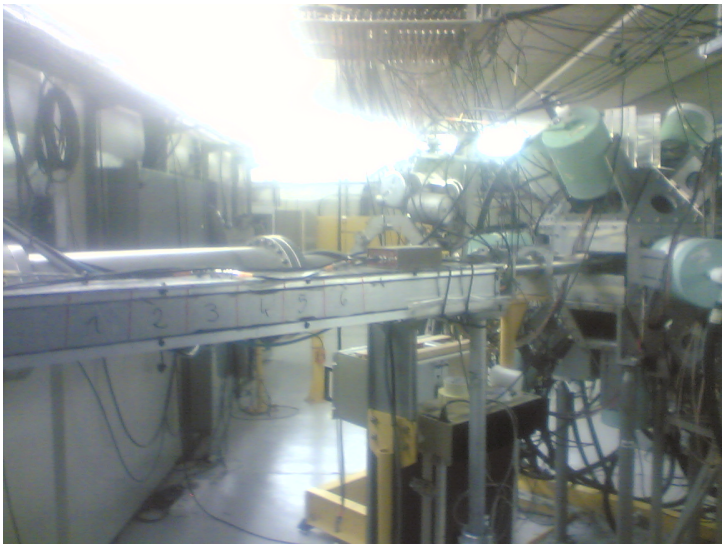

Figure 5.5: One of the neutron detector set-ups in coincidence with the AFRODITE array for time-of-flight measurements

5.5.3 Setup for the Proposed Fast Neutron Detectors Test Experiment

The proposed experiment for testing the neutron detectors in this project was to use the (^{3}He,n) two proton stripping reaction and nine neutron detectors. The nine neutron detector setup was to be used to measure fast neutrons emitted in the reaction. A proposal was submitted and accepted by the PAC of iThemba LABS under PR160, see Appendix B. The neutron detectors were

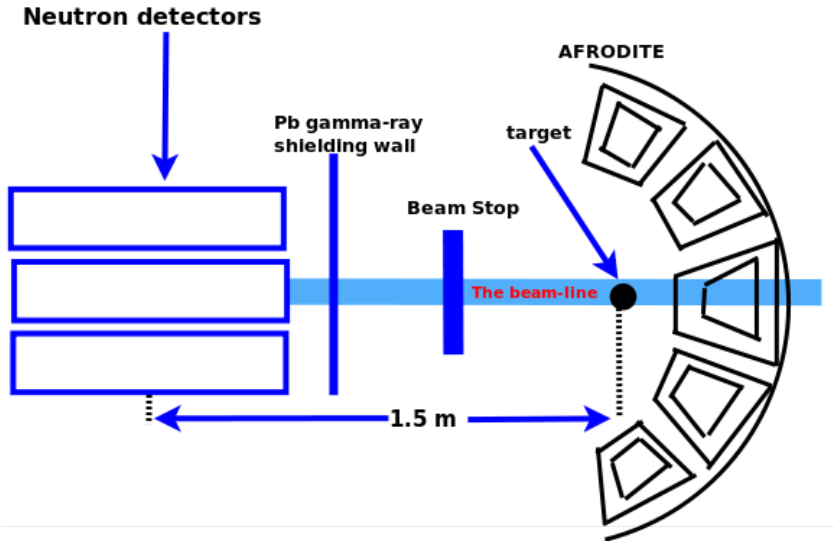

Figure 5.6: Schematic set-up for (^{3}He,n) experiments

positioned about 1.5 m downstream from the target so that they detected neutrons at and close to 0°. The beam was caught on a bismuth beam stop, about 0.5 m behind the target which was placed at the centre of the AFRODITE. A wall of lead shielded the neutron detectors from γ-rays from the target. In order to achieve good detection efficiency for fast neutrons, the detector was positioned lengthwise, parallel to the beam pipe. Nine detectors were to be positioned with the central detector placed along the beam axis as, shown in Fig. 5.6.

In order to acquire experience with the neutron detection system, we used two time-of-flight measurements as described in sections 5.5.1 and 5.5.2. The major difference between these two measurements and the complete setup was the volume of the plastic neutron detector and the ion beam. In the complete detection system, we expected to obtain more detection efficiency because of the use of a large volume of scintillating plastic.

Chapter 6 - Results and Discussion

6.1 The ^{232}Th$(\alpha, x\mathrm{n})$ Reaction Test Result

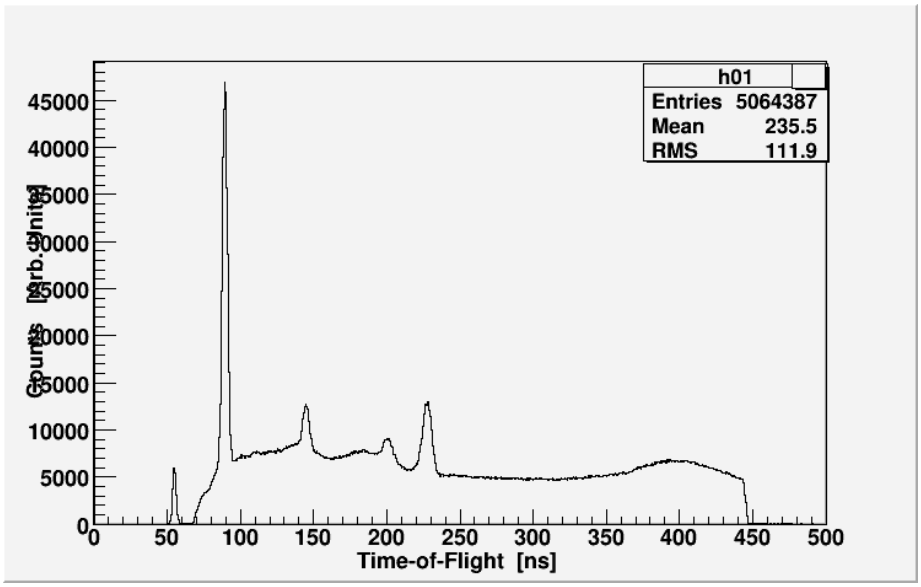

Figure 6.1: Time-of-flight spectrum obtained from the ^{232}Th$(\alpha, x\mathrm{n})$ reaction test.

The ^{232}Th$(\alpha, x\mathrm{n})$ reaction with 42 MeV bombarding energy was used to test the neutron detector with the time-of-flight technique as described in section 5.5.1. As illustrated in Eq. 1.2.1, section 1.2 the residual nuclei in this reaction were $^{236-x}$U (mainly ^{232}U). This reaction selected by S. S. Ntshangase *et al.*, for studying the electric dipole moments in ^{230,232}U nuclei [34]. Statistical neutrons from these fusion evaporation reactions, fast neutrons from the direct reaction and fast neutrons from fusion fission were therefore expected to be detected.

Time-of-flight, energy and position spectra were generated to show the ability of the neutron detector to distinguish between neutron and γ rays from different sources. Fig. 6.1 shows a time-of-flight spectrum where the different peaks represent neutrons and γ-rays.

To identify the particles, and as it had been predicted from the Monte Carlo

simulations, the spectrum which included the time-of-flight versus the position was generated. Fig. 6.2 shows the position versus time-of-flight spectrum, which is close to the spectrum illustrated in Fig. 6.5 obtained from the simulations. The fast neutrons appear at the time of 200 and 225 nano-seconds whereas the statistical neutrons were found in the range of 340 to 440 nano-seconds. The γ-rays from the target and the beam dump in this spectrum corresponded to the 85 and 145 nano seconds peaks respectively. Regarding

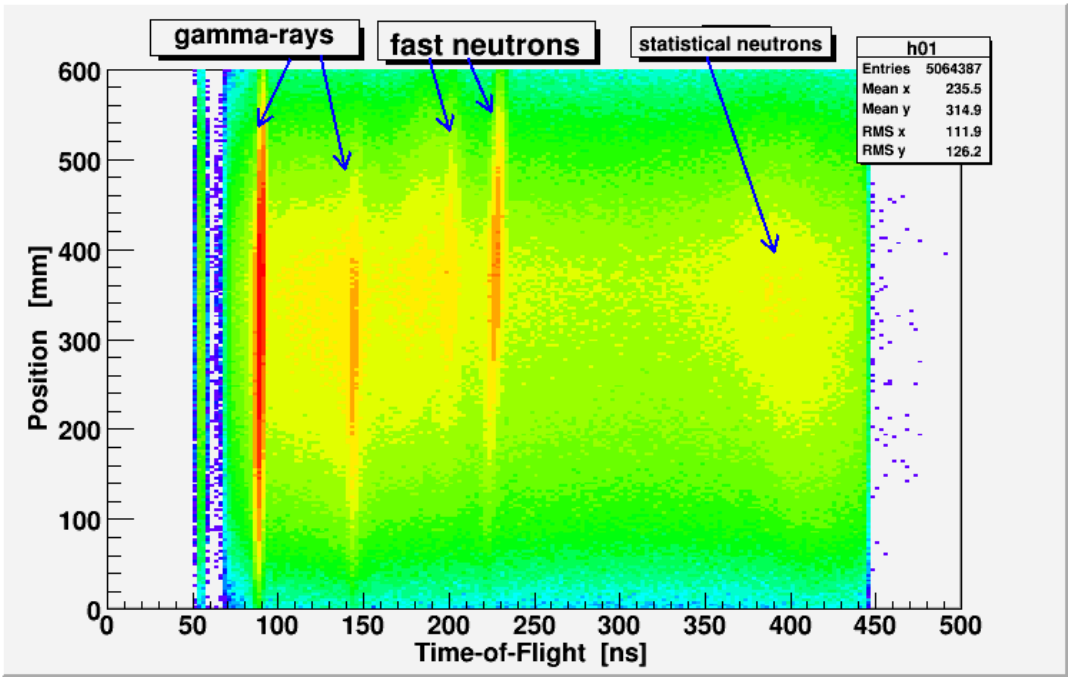

Figure 6.2: The position versus time-of-flight scatter plot.

the energy distribution, Fig. 6.3 shows the energy versus time-of-flight matrix; the energy lumped around 200 nano-seconds. This lump can be explained in terms of the fast neutron peak. The γ-ray pulse heights are shown in the energy range of 0 to 4 MeV and the muon cosmic ray pulse height at 20 MeV.
Since the plastic scintillation neutron detector measures only the energy of the recoil ^{1}H(n,p) reaction, the full energy of the neutron was not always deposited within the detector volume. The measured energy can be a lower energy than the incident energy of the neutron. It can also appear higher because of the resolution (the plastic scintillation detector has poor energy resolution). Fig. 6.4 shows the energy spectrum obtained from the neutron detector. The first peak in this spectrum corresponds to γ-rays coming from different sources and the second peak corresponds to the fast neutrons as described in this figure. The energy deposited by muon cosmic rays is approximately 20 MeV.

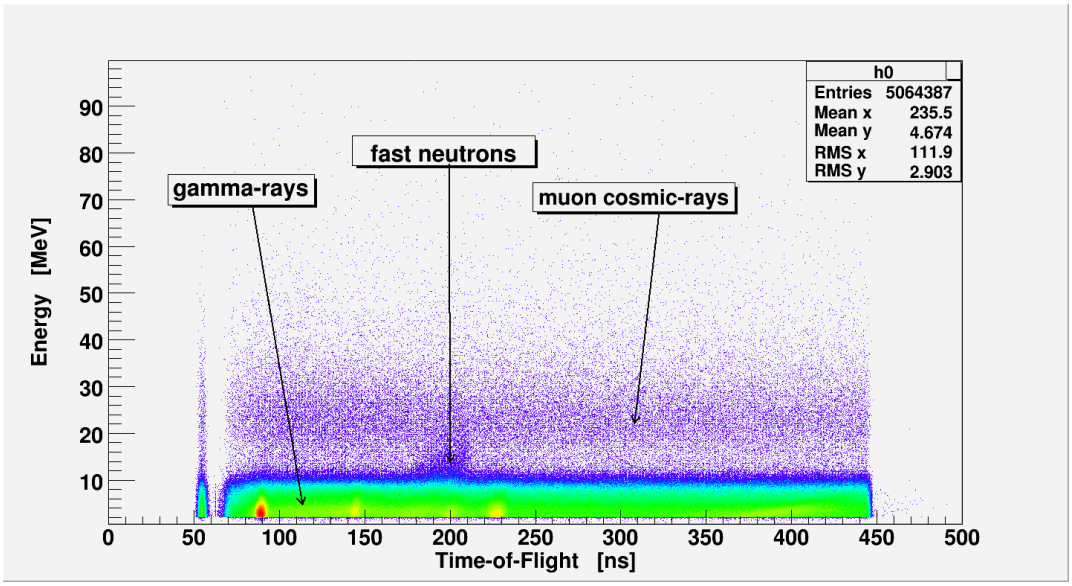

Figure 6.3: The energy-time of flight matrix.

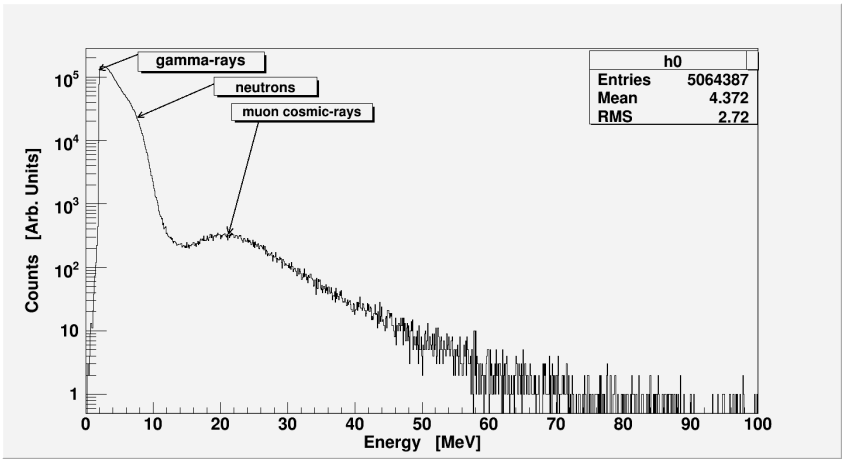

Figure 6.4: The energy spectrum obtained from the neutron detector.

6.2 Comparison with Simulation Results and Particle Identification

As described in section 4.6 the results of the Monte Carlo simulations can be used to interpret the time spectrum of the large-volume neutron detector according to the time-of-flight technique. The simulated time-of-flight spectrum presented in Fig. 4.4 is very close to the measured time-of-flight spectrum showed in Fig. 6.1. Both of the spectra show the time-of-flight structure corresponding to the fast statistical neutrons and γ-rays from different sources. The simulated matrix of the position versus the time-of-flight (Fig. 6.5) com-

pares fairly well to the measured one (Fig. 6.2). In both matrices the straight lines (3 lines in Fig. 6.5 and 2 lines in Fig. 6.2) represent the γ rays coming from the collimator, the target and the beam dump, whereas the other two lines showing slight distortion (tilt) represent the fast neutron. Since the aim of this project was to test the capability of the large-volume neutron detector to distinguish between the fast neutrons from the statistical neutrons and γ-rays, these Monte Carlo simulations successfully assisted to identify the particles and achieve this task.

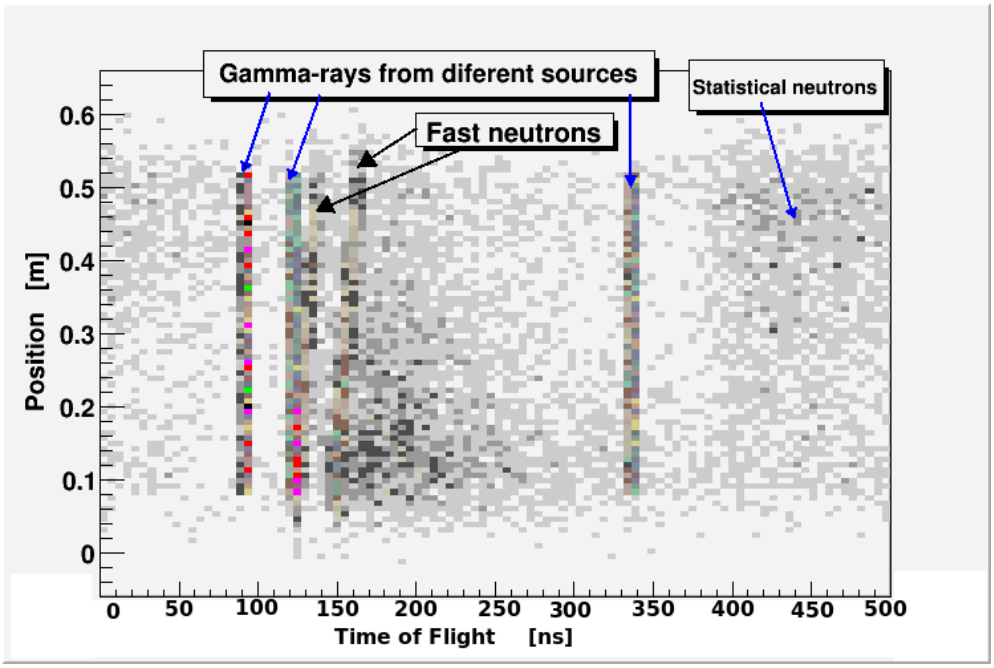

Figure 6.5: The simulated position versus time-of-flight matrix. This figure is a duplicate of Fig. 4.5 for clarity.

6.3 The ^{152}Sm(^{12}C,xn) Reaction Test Result

As it presented in Eq. 1.2.2 section 1.2, we used the ^{152}Sm(^{12}C,xn) reaction with a 64 MeV ^{12}C ion beam to test the neutron detector. The ^{152}Sm target had a thickness density of 5.0 m g/cm^2. Since the atomic ion beam (^{12}C) in this reaction is relatively heavy, we did not expect to see fast neutrons in this reaction test. Table 6.1 shows the calculated evaporation residue cross-section produced in the (^{12}C +^{152}Sm) reacton at 64 MeV. According to this calculation, statistical neutrons were expected to be seen in this experiment. The maximum cross-section was found in the 4 neutron evaporation channel population. This residue nucleus had a mass number (A) of 160 and an atomic number (Z) of 68, which is the ^{160}Er$_{68}$ nucleus for which the cross-section is 867.3 mb. Fig. 6.6 shows the energy spectrum of the neutrons at forward

Z	A	Cross section per residual nucleus [mb]
68	164	0.0
68	163	3.0
68	162	3.0
68	161	34.6
68	160	867.31
68	159	97.4
68	158	0.0

Table 6.1: The calculated evaporation residues cross-section for the ^{12}C+^{152}Sm reaction is dominated by the ^{152}Sm(^{12}C,4n) channel.

angles which predicts a peak at 1.5 MeV. After this peak an exponential decay of the statistical neutrons is expected.

As described in Chapter 5 section 5.5.2 the neutron detector was set-up in coincidence with the AFRODITE array detectors. The following figures show the result of this test. Fig. 6.7 shows the time difference spectrum, which is the difference between the time signal obtained from the HPGe Clover detector and the time signal obtained from the neutron detector. In this spectrum, the statistical neutron data appear to be in the range of 750 to 900. Fig. 6.8 shows the energy spectrum obtained from the HPGe Clover detector with a γ-n trigger. The γ-ray energy transitions for ^{160}Er$_{68}$ and ^{161}Er$_{68}$ residual nuclei are populated as predicted from the statistical model code calculation. This implies that, four and three statistical neutrons are produced respectively in this test reaction from the compound nucleus ^{164}Er$_{68}$. The cross section is dominated by ^{160}Er in the γ spectrum as predicted by the CASCADE calculation. The very interesting point in this spectrum concerns the energy transitions at 121.5 and 244.7 keV, which correspond to the Coulomb excitation process. A part of the kinetic energy of the ^{12}C ion beam is transferred to the ^{152}Sm

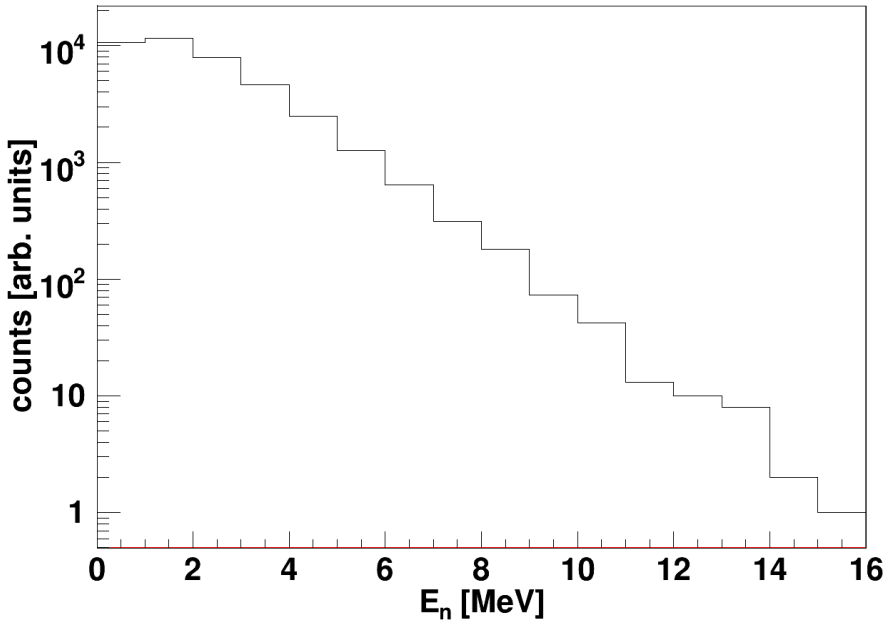

Figure 6.6: The energy spectrum of the neutrons at forward angles calculated with the Cascade code [35].

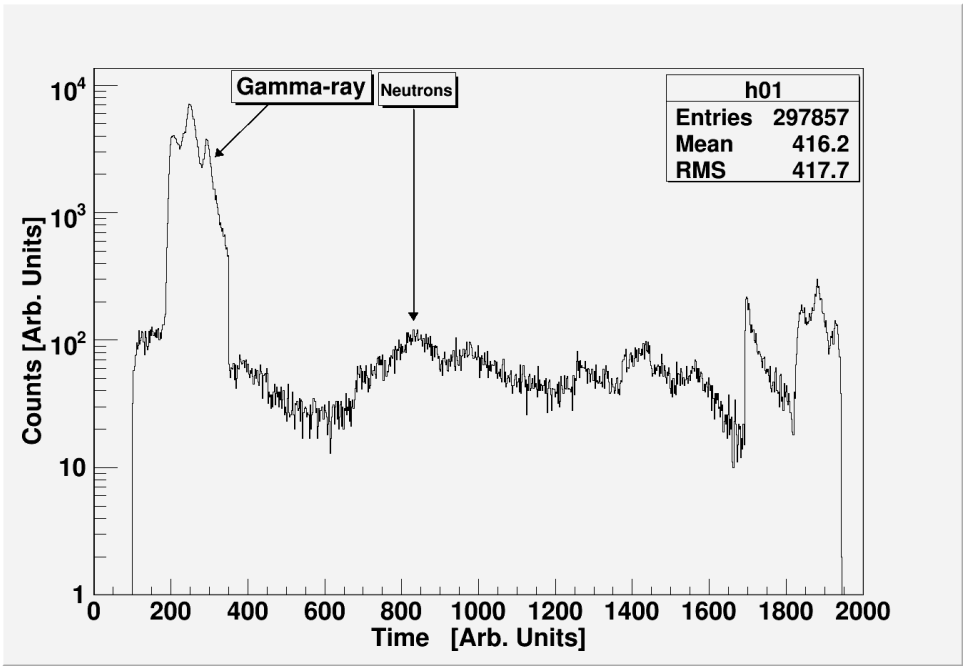

Figure 6.7: Time difference between the time recorded from the HPGe Clover detector and the neutron detector.

target nuclei through electromagnetic interaction.
Fig. 6.9 shows the same spectrum illustrated in Fig. 6.8, but selecting the events in the (750 to 900 channels) time gate corresponding to the statistical neutrons as showed in Fig. 6.7. By using this gate the energy transition 244 keV does not appear and the 121.5 keV is reduced. These transitions are not fully eliminated but their reduction indicates that neutrons and gamma particles are detected in coincidence enhancing the intensity of the gamma rays originating from fusion evaporation in comparison to the gamma rays from Coulomb excitation where the emission of a neutron is unlikely. As neutrons are not emitted in coulomb excitation (only γ-rays) 121.5 and 244 keV transitions could not be seen when a neutron was required to be detected. The 121.5 keV transition is seen but is reduced and 244 keV transition is significantly reduced but still present, if viewed on an enlarged plot.

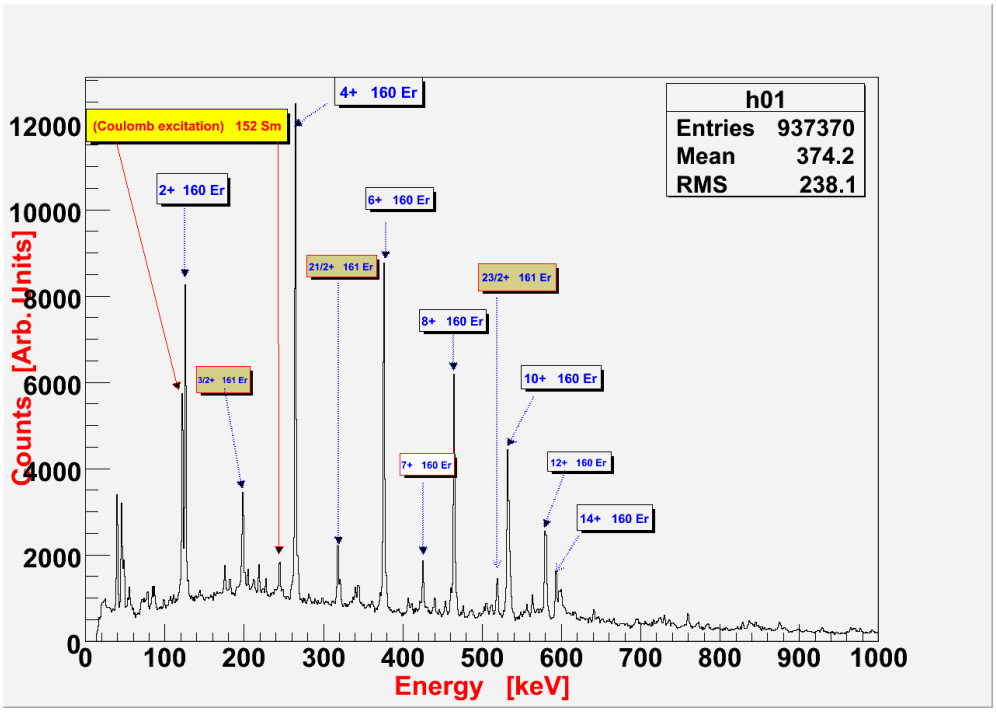

Figure 6.8: The total energy projection spectrum obtained from the HPGe Clover detector.

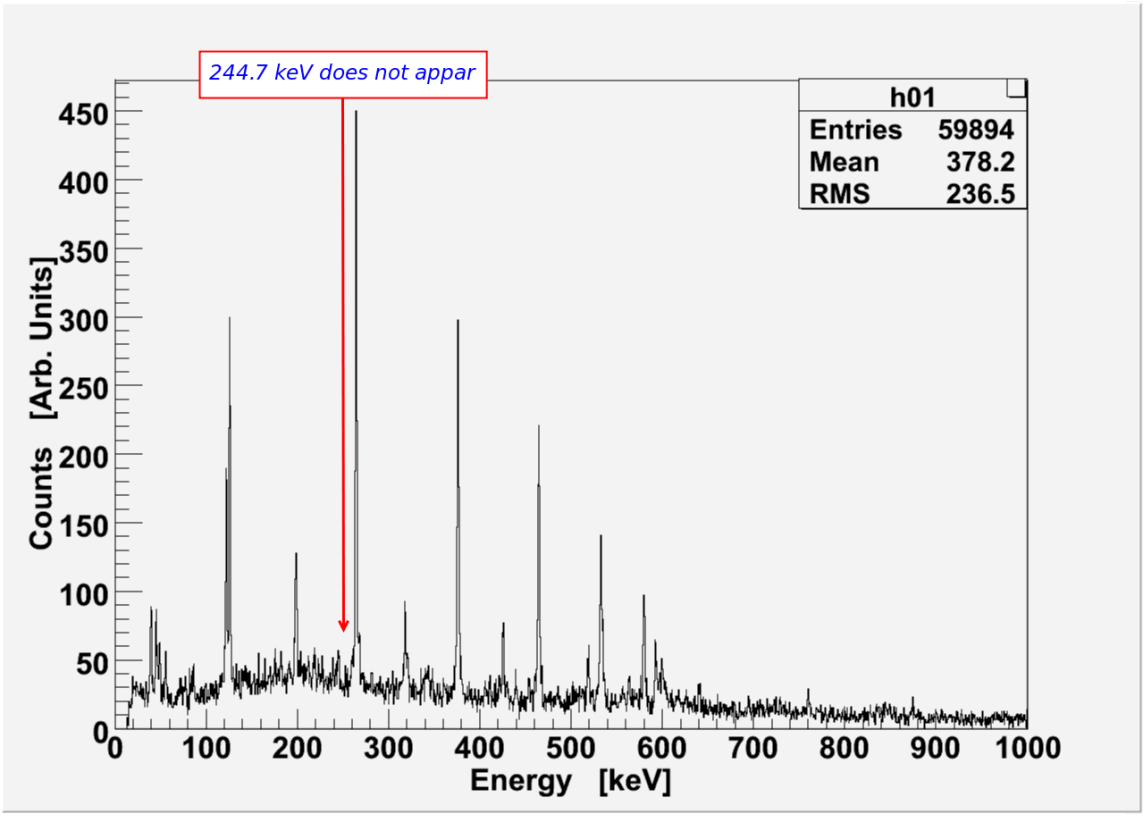

Figure 6.9: The energy spectrum obtained from the HPGe Clover detector using (750-900) time difference gate.

Chapter 7 - Conclusion and Future Work

7.1 Conclusion

Nine 100x100x600 mm^3 plastic scintillators, formerly built for the neutron time-of-fight measurements at iThemba LABS, were refurbished. These detectors are now ready to be used as an ancillary detector array with the AFRODITE gamma ray spectrometer. The interaction point in the detector was deduced from the relative amplitude at both ends of the detector measured by means of two individual photomultiplier tubes. The position resolution of these detectors was determined using muon cosmic rays selected with two additional detectors set in coincidence. A position resolution of $\sim$ 4.3 cm (FWHM) on average along the detector was determined.
Two measurements were performed to test the ability of these detectors to distinguish between neutrons with a wide range of energy, and γ-rays. The ^{232}Th$(\alpha, x$n) reaction test was performed using one of the neutron detectors and the time-of-flight technique, whereas the ^{152}Sm(^{12}C,xn) reaction test was performed using the coincidence technique. The measurements were performed at iThemba LABS using 42 MeV α particles as an ion beam and ^{232}Th as target nuclei for the time-of-flight measurement, and the ion beam was ^{12}C incident on ^{152}Sm target nuclei at E_{lab} = 64 MeV for the coincidence measurement.
Using the time-of-flight technique, fast neutrons produced in the ^{232}Th$(\alpha, x$n) reaction test were detected and separated from the statistical neutrons and γ-rays. Statistical neutrons from fusion evaporation reactions were produced in ^{152}Sm(^{12}C,xn) fusion evaporation reactions. Indication of correlated neutrons and gamma rays detected with the neutron detector and the AFRODITE γ-ray spectrometer, respectively, was observed through the reduction of the Coulomb excitation in neutron gated spectra. Monte Carlo simulations were performed to predict the time spectrum of the neutrons emitted in nuclear reactions. These simulations were aimed at anticipating the separation of statistical neutrons from fusion evaporation, and prompt and uncorrelated γ-rays from the fast neutrons emitted in the ^{232}Th$(\alpha, x$n) reaction. The simulation provided a relative prediction of the measured time-of-flight spectrum.

7.2 The Future Work

For the future, the proposed test experiment as described in section 5.5.3 is expected to be performed in 2011. A large-volume plastic scintillator detection array, (3x3) configuration is to be used to select the ^{152}Sm(^{3}He,n)^{154}Gd two-proton stripping reaction to obtain very selective data. If successful, many interesting experiments may become possible, for instance the search for the 0^+ states at the bottom of super-deformed bands. The study of the systematics of two-proton structures in nuclei in the N=88 and 99 region should also be possible. There is also evidence that second vacuum structures exist in the deformed Ce nuclei with 8 protons outside the closed Z = 50 shell (see section B.2 of Appendix B). These 0^+-states should be populated in the (^{3}He,n) reaction.
The proposed experiment for testing the neutron detectors in this project was to use the (^{3}He,n) two proton stripping reaction and nine neutron detectors. The nine neutron detector setup was to be used to measure fast neutrons emitted in the reaction. A proposal was submitted and accepted by the PAC of iThemba LABS under PR160. The neutron detectors were be positioned about 1.5 m downstream from the target so that they detected neutrons at and close to 0°. The beam was caught on a bismuth beam stop, about 0.5 m behind the target which was placed at the centre of the AFRODITE. A wall of lead shielded the neutron detectors from γ-rays from the target. In order to achieve good detection efficiency for fast neutrons, the detector was positioned lengthwise, parallel to the beam pipe. Nine detectors were to be positioned with the central detector placed along the beam axis as, shown in Fig. 5.6.
In order to acquire experience with the neutron detection system, we used two time-of-flight measurements as described in sections 5.5.1 and 5.5.2. The major difference between these two measurements and the complete setup was the volume of the plastic neutron detector and the ion beam. In the complete detection system, we expected to obtain more detection efficiency because of the use of a large volume of scintillating plastic.

Appendix A - The Python Code

The python code used for the time-of-flight simulations:

```
from visual import *
from time import clock
from visual.graph import *
from random import random
from pylap import *
from math import *


#
# The geometry of the experiment
# 0.20
# 3  1.29                0.58
#
# 0     0.2     1.6         4.6
# coll  targ    detector    beam dump
#

dbeam = []
dpart = []

dbeam.append(0.0)  # coll
dbeam.append(0.2)  # target
dbeam.append(1.6)  # beam dump

dpart.append(1.6)
dpart.append(1.4)
dpart.append(2.4)


########################################
# initialization
########################################
```

```
# define the lists and couple of variables

Nevents = 10001
Ntotevents = 0
i = 0
j = 0
data0 = []
data1 = []
data2 = []
data3 = []

amu = 931.1
c = 3.e8 # light speed in [m/s]

Ebeam = 42.0    # MeV   ###### (The beam energy)
Ab = 4.0
Mn = amu + 8.   # Neutron mass in [MeV]
vbeam = c*(2*Ebeam/Ab/amu)

timeshift= 90.e-9 #ns
# Define the size and distances

D = 1.28    # [m] [[128-> Detector->Target] , [58-> Detector->Beam dump ] # cm
L = 0.6     # [m] [156-> Detector length    , [60+30+30+18+18]           ] # cm
DL = D + L  # [m] [217-> Collimator->Target , [345-> Collimator->Detector] # cm
W = 0.1     # [m]
H = 0.1     # [m]

TrackIn = 0.
TrackOut = 0.
# work out the maximum theta covered by the detector to generate
# uniformly the neutrons towards the detector only
TheM = (W*W + H*H)**0.5/2./D # [rad]
a = 1./(1.-cos(TheM))

# cross sections plus a couple of constants

nat = 4.2e22
Lambda = nat*0.2e-24
Lambda=100.*Lambda # atom/[m]

LambdaN=nat*1e-24*100.
```

```
Efastn = 10.###########    11.0  or 30.0

# Defines some limits for the displays at the end

Rt = 600.
tmin = 0.
tmax = Rt*1.e-9
emin = 0.
emax = 30.0


wraparound = 500.e-9 #ns

# Gaussian random number generator

def Gaus(mean, fwhm):
   sigma=fwhm/2.35
   y = random()
   if y == 0:
       y = random()
   z = random()
   x = z * 6.283185
   result = mean + sigma*sin(x)*(-2*log(y))**0.5;
   return result


########################################
# Start with the simulation
########################################


# Neutrons

while j < Nevents:

    test = 0

    while test <1:

#   choose the target(collimator, target or beam dump)
        pos = int(3.*random())

#   point on a sphere (or at least part of it)
        theta = a*acos(random()*TheM)
```

```
        phi = random()*2.*pi

        x = sin(theta)*cos(phi)
        y = sin(theta)*sin(phi)
        z = cos(theta)

        norm1=dpart[pos]/z

        x1=norm1*x
        y1=norm1*y
        z1=norm1*z

#   Test if the particle enters the detector

        if z > 0. and abs(x1) < W/2. and abs(y1) < H/2.:


            norm2=(dpart[pos]+L)/z
            x2=norm2*x
            y2=norm2*y
            z2=norm2*z

#       Test if the particle exits from the back end
            if abs(x2) > W/2. or abs(y2) > H/2.:

#           Test if the particle exits from the walls
                if abs(y) < abs(x):
                    norm2 = W/2./abs(x)

                else:
                    norm2 = H/2./abs(y)

                x2=norm2*x
                y2=norm2*y
                z2=norm2*z

#       Work out the effective thickness

            TrackIn = (x1*x1 + y1*y1 + z1*z1)**0.5
            TrackOut = (x2*x2 + y2*y2 + z2*z2)**0.5
            EffecThick = TrackOut - TrackIn


#       Generate the neutron energy
```

```
            if random() < 0.5 and pos < 2:
                En = Gaus(Efastn,2.0)
            else:
                En = -log(random())/0.35
#    work out the cross section event by event (we assumed
#    a constant cross section but it is not true. Sigma is inversly
# proportional to v
            v = (2.*En/Mn)**0.5
            Lambda=LambdaN*0.05/v
            v=v*c

#       Work out the interaction point
            InteracPoint = -log(random())/Lambda
            if InteracPoint < EffecThick:
                test = 1 # to exit the while loop

#       -> The neutron entered and interacted in the detector, we now carry on

#   Work out the theoretical time of flight

    tof = (dpart[pos] + InteracPoint)/v + dbeam[pos]/vbeam + timeshift
    while tof > wraparound:
        tof = tof - wraparound
    tof = wraparound - tof
    if pos == 2:
        InteracPoint = L - InteracPoint

#   Work out the Energy spectrum from experimental measurement
    tof = abs(Gaus(tof,2.e-9)) #3ns of time resolution
    Dn = Gaus(dpart[pos] + InteracPoint,0.1) # 10cm position resolution
    data2.append(En) #Input energy
    En = 0.5*Mn*(Dn/tof/c)**2
    data3.append(En) # Measured energy

    data0.append(Dn-dpart[pos]) # position in the detector
    data1.append(tof) # measured tof

    j+= 1 # Increment the event number for the main while loop
    Ntotevents += 1

##########
# Generate some gammas from the different sources
##########
```

```
j = 0

while j < Nevents:

    pos = int(3.*random())
    tof = (dpart[pos]+L*random())/c + dbeam[pos]/vbeam+ timeshift
    tof = abs(Gaus(tof,2.e-9)) # Measured energy
    while tof > wraparound:
        tof = tof - wraparound
    tof = wraparound - tof
    Eg = -log(random())/1.0
    data2.append(Eg) #Input energy
    data3.append(abs(Gaus(Eg,Eg/4.))) # Measured energy

    data0.append(L*random()) # position in the detector
    data1.append(tof) # measured tof

    j+= 1 # Increment the event number for the main while loop
    Ntotevents += 1

########################################
# plot the results
########################################


vdist1 = gdisplay(x=0,
             width=600, height=250, xtitle='tof [ns]', ytitle='N')

d=(tmax-tmin)/Rt
timen = ghistogram(bins=arange(tmin,tmax,d),
                        accumulate=1, average=0, color=color.red)
timen.plot(data=data1)

vdist2 = gdisplay(x=0,y=250,
             width=600, height=250, xtitle='E Th [MeV]', ytitle='N')

d=(emax-emin)/Rt
energyTh = ghistogram(bins=arange(emin,emax,d),
                        accumulate=1, average=0, color=color.green)
energyTh.plot(data=data2)

vdist3 = gdisplay(x=0,y=500,
             width=600, height=250, xtitle='E Exp [MeV]', ytitle='N')
```

```
energyExp = ghistogram(bins=arange(emin,emax,d),
                       accumulate=1, average=0, color=color.cyan)
energyExp.plot(data=data3)

print j

############################################################
# Make a 2D scatterplot of time of flight versus position
############################################################

NPos = 100
NTof = 100
YPos = 0
XTof = 0

#initialize the list
TwoD = []
rgb = []
rgb.append(0.)
rgb.append(0.)
rgb.append(0.)
maxi = 0.

for i in range(NPos*NTof):
    TwoD.append(0.)

# fill a table
for i in range(Ntotevents):
    if data0[i] < 1.0:
        YPos = int(100*data0[i]+20)
        XTof = int(100*data1[i]/wraparound)
        TwoD[YPos*100+XTof] += 1
        if maxi < TwoD[YPos*100+XTof]:
            maxi = TwoD[YPos*100+XTof]

#plot the 2D spectrum
for i in range(NTof):
    x = i-NTof/2
    for j in range(NPos):
        y = j -NPos/2
        rgb[0]=0.
        if TwoD[j*100+i] > 0:
            rgb[0]=TwoD[j*100+i]/maxi*2./3.+1./3.
        box(pos=(x,y,0),length=1.0, height=1.0, width=0.2, color=rgb)
```

```
########################################
#Generate a 2D scatterplot in ROOT format
########################################

filename = open("Fridaynow3.C", "w")
filename.write("{\n")
filename.write("//=========Macro generated from Python\n")
filename.write("   TCanvas *c1 = new TCanvas(\"c1\", \"c1\",358,51,700,500);\n")
filename.write("   c1->Range(-1,-0.625,9,0.625);\n")
filename.write("   c1->SetBorderSize(2);\n")
filename.write("   c1->SetFrameFillColor(0);\n")
filename.write("   TH1 *h02 = new TH2F(\"h02\",\"\",98,0,")

value = wraparound
s = str(value)
filename.write(s)
filename.write(",98,")
value = -0.1*L
s = str(value)
filename.write(s)
filename.write(",")
value = 1.1*L
s = str(value)
filename.write(s)
filename.write(");")
filename.write("\n")

for i in range(100):
    for j in range(100):
        if TwoD[j*100+i] > 0:
            value = 'h02->SetBinContent('
            s = str(value)
            filename.write(s)
            value = j*100+i
            s = str(value)
            filename.write(s)
            value = ','
            s = str(value)
            filename.write(s)
            value = TwoD[j*100+i]
            s = str(value)
            filename.write(s)
            value = ');'
```

```
            s = str(value)
            filename.write(s)
            filename.write("\n")


#   TPaveStats *ptstats = new TPaveStats(0.78,0.755,0.98,0.995,"brNDC");
#   ptstats->SetName("stats");
#   ptstats->SetBorderSize(2);
#   ptstats->SetFillColor(19);
#   ptstats->SetTextAlign(12);
#   TText *text = ptstats->AddText("h02");
#   text->SetTextSize(0.0368);
#   text = ptstats->AddText("Entries = 5064387");
#   text = ptstats->AddText("Mean x =  3.709");
#   text = ptstats->AddText("Mean y = -0.06674");
#   text = ptstats->AddText("RMS x =  2.238");
#   text = ptstats->AddText("RMS y = 0.1239");
#   ptstats->SetOptStat(1111);
#   ptstats->SetOptFit(0);
#   ptstats->Draw();
#   h02->GetListOfFunctions()->Add(ptstats);
#   ptstats->SetParent(h02->GetListOfFunctions());

filename.write("   h02->Draw(\"col\");\n")
filename.write("   c1->Modified();\n")
filename.write("   c1->cd();\n")
filename.write("   c1->SetSelected(c1);\n")
filename.write("  }\n")

filename.close()
```

Appendix B - The Proposal of the (^{3}He,n) Experiment
P. Papka *et al.*

RESEARCH PROPOSAL TO iTHEMBA LABS: PHYSICAL SCIENCES RESEARCH PROGRAMME ON SSC FACILITY
Date: 29 September 2009

ABSTRACT

We intend to use large volume neutron detectors and time-of-flight to distinguish between fast neutrons from (^{3}He,n) direct reactions and statistical neutrons from (^{3}He,xn) fusion-evaporation reactions. The neutrons will be measured in coincidence with AFRODITE to search for excited 0^+ states in the residual nucleus.
We request two weekends to test the system using the ^{152}Sm(^{3}He,n)^{154}Gd reaction at a beam energy of 22.5 MeV.

EMPHASIS

(a) Pure basic research 50%
(b) Direct basic research
(c) Applied research
(d) Experimental development, services 50%

B.1 INTRODUCTION

Direct reactions give very specific and selective information on the properties of nuclear levels. This has been exploited extensively with high resolution (magnetic) spectrometers when the outgoing particle is charged such as, the proton, α and β-particles which respond to electromagnetic field. An example showing a spectrum from the ^{152}Gd(t,p)^{154}Gd reaction [1] is shown in Fig. 1.1.

In this spectrum the largest peaks below 2 MeV excitation energy in ^{154}Gd are the 0^+ states. The angular distributions for these states are strongly forward peaked with the maximum of the differential cross-section at 0^o, characteristic of L=0 transitions, this means that the pair of neutrons have been stripped from the projectile nucleus simultaneously with their spins paired off to angular momentum zero.

Reactions where protons are stripped of the beam nucleus, so that the outgoing particle is a neutron, are difficult to carry out especially to obtain sufficient neutron energy resolution. Examples of these neutron emitting direct reactions are *(d,n)* and *(^{3}He,n)* which donate one and two protons to the target nucleus respectively. One proton stripping can be made with the (^{3}He,d) reaction, but two proton stripping requires reaction using heavy ions such as (^{16}O,^{14}C) and very good resolutions are still difficult to achieve. A search of the BNL Nuclear Data references has only 7 references with (^{3}He,n) in the title of the paper for the years 1990 to 2009. Most of the references are to papers on Astrophysical measurements.
We propose to use large plastic neutron detectors, to give efficiency, time-of-flight to separate fast $\sim$ 27 MeV neutrons from statistical fusion-evaporation neutrons with energies of less than 6 MeV and coincidences with γ-rays detected in AFRODITE to give excellent resolution.

B.2 POSSIBLE FUTURE EXPERIMENTS

If this apparatus proves to be sufficiently powerful, there are many experiments that might become possible. We list a few spring to mind:

{*a*} Search for the 0^+ states at the bottom of Superdeformed bands:
Stable isotope targets to be used with the (^{3}He,n) reaction to populate nuclei containing known Sd bands are ^{147,148}Sm and ^{192}Pt to search ^{149,150}Gd and ^{194}Hg respectively.The abundances of ^{147,148}Sm are 15 % and 11 % respective, but ^{192}Pt is only 0.8 % abundant. However ^{194}Hg is the best candidate for finding 0^+ states related to SD as there are 3 SD bands known down to spin 10^+ and the decay out of the bottom of the band is known so that its excitation energy is known exactly. The SD nuclei ^{149,150}Gd are more difficult inspite of having easily obtainable targets. Their SD bands decay out at about spin 30 making extrapolation down to 0^+ very uncertain. But the high-j configurations of the SD bands for ^{149,150}Gd are $(\pi i_{13/2})^2$ $(\nu j_{15/2})^1$ and $(\pi i_{13/2})^2$ $(\nu j_{13/2})^2$ respectively. Thus it would help the understanding of these structures to discover if the $(\pi i_{13/2})^2$ states can be observed at low spin using the (^{3}He,n) reaction.

{*b*} If the proposal made here is successful, it will obviously be informative to examing the systematics of two proton structures in other nuclei in the

N=88 and 90. Also much might be learned by using the (^{3}He,n) reaction to study structures in odd nuclei in this region.

{*c*} There is evidence that second vacuum structures exist in the deformed Ce nuclei with 8 protons outside the closed z=50 shell. These structures arise due to the proton [404]9/2$^+$ orbit being at the Fermi surface. These 0$^+$ states should be populated in the (^{3}He,n) reaction. The only nucleus that can be reached with a stable target is ^{132}Ce , also with well known SD bands, via the (^{3}He,n) reaction. Complications arise dealing with ^{130}Ba material counting only 0.1 % of natural Ba.

{*d*} Mirror nuclei, across the N=Z diagonal, can be studied using the (^{3}He,n) reaction up to ^{42}Ti.

B.3 EXPERIMENTAL TECHNIQUES AND EQUIPMENT

B.3.1 APPARATUS

Twelve large neutron detectors were used [2] at the then NAC in the 1990s to study Gamow-Teller strengths in (p,n) reactions at 122 MeV. Fig. 3.3 shows a schematic of the neutron detectors [2]. Currently 9 of these detectors are at the University of Stellenbosch being refurbished. Each detector consists of a 600x100x100 mm^3 rectangular bar of NE 102A scintillator. Two conical perpex (or PVC) light guide, at either end of the bar, transport the scintillation light to the two Hamamatsu R329 photomultiplier tubes (Fig. 3.3). Typical time resolution achieved with these detectors was 1.5 ns.

In Fig. B.1 we show a schematic layout of the experimental set-up. The neutron detectors will be positioned about 1.5 m down-beam of the target so that they detect neutrons at and close to 0°. The beam will be caught on a bismuth beam stop, about 0.5 m, behind the target at the center of AFRODITE. A wall of lead will shield the neutron detectors from γ-rays from the target. In order to achieve a good detection efficiency for fast neutrons, the detector will be positioned lengthwise parallel to the beam pipe. Having photomultipliers at both ends of the detectors gives a degree of position resolution, improving the t-o-f resolution of the experimental geometry. Nine detectors will be positioned with the center detector placed along the beam axis as shown in Fig. B.2. In this configuration the detectors will be positioned at an angle of 4.0° and will each subtend about 3.5° to target. About 50 per cent of l=0 neutrons from the (^{3}He,n) reaction should hit the detectors.

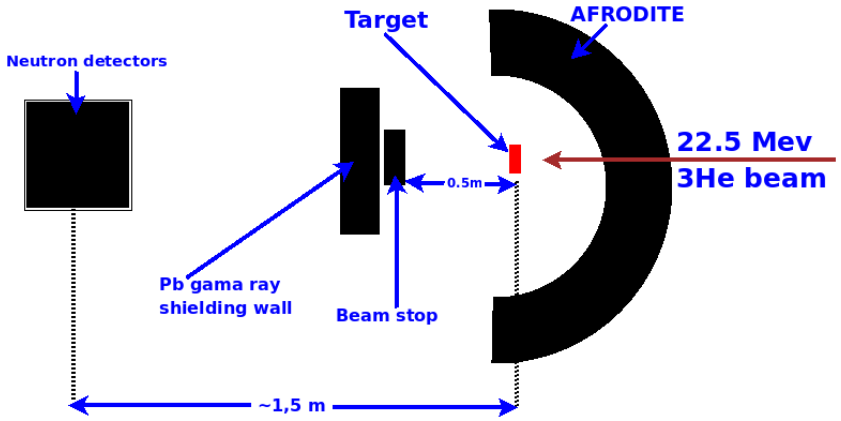

Figure B.1: Schematic set-up for (^{3}He,n) experiments

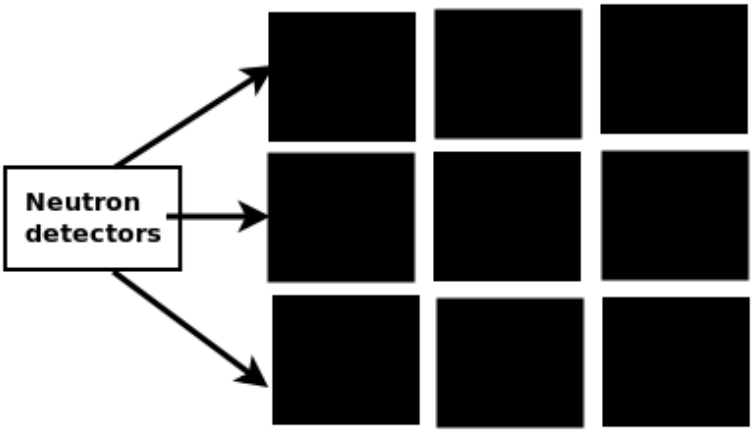

Figure B.2: Beam view of arrangement of neutron detectors

B.3.2 Reaction Selection

The Q-values for the (^{3}He,n) reaction on ^{152}Sm are:
1n=> +5.802 MeV
2n=> -2.855 MeV
3n=> -9.341 MeV
4n=> -17.938 MeV
The ^{3}He Coulomb barrier is at 17.74 MeV for ^{152}Sm and at 22.42 MeV for ^{209}Bi beam stopper.
Pace4 predicts that the fusion-evaporation reaction yields and cross-section;
^{153}Gd 5.7 per cent 29 mb (2n)
^{152}Gd 93 per cent 463 mb (3n)
^{151}Gd 0.4 per cent 2.2 mb (4n)

with a maximum partial wave cross-section at $5.5\hbar$.
Evaporation neutron yields peak below 2 MeV and are less than 1 % of maximum at 6 MeV. 6 MeV neutrons have a velocity of 34 mm/ns (v/c=11.3 %) taking $\sim$ 50 ns to travel the 1.5 m. The majority of the statistical neutrons will take $\sim$ 100 ns to travel the 1.5m.
With a Q-value of +5.802 MeV for the (^{3}He,n) reaction, these direct reaction neutrons will have an energy, when populating excited states, of about 25 MeV, a velocity of 69 mm/ns (v/c=23 %) taking 22 ns to travel 1.5 m. Any residual (γ-flash) from the target, getting through the Pb shielding, will take $\sim$ 5 ns to travel 1.5 m. Thus the γ-rays, fast neutrons from the direct (^{3}He,n)reaction and statistical neutrons from (^{3}He,xn) reactions will be well separated by time-of-flight even over the relatively short distance of 1.5 m and even for reactions with Q-values down to zero MeV. It should be remembered that the statistical neutrons are emitted isotropically in the slow moving centre-of-mass, whereas the L=0 neutrons from (^{3}He,n) reactions have most of their cross-section peaked within 10 degree of 0 degree. The neutron detectors will subtend a small solid angle to the statistical neutrons of about 1 % of 4π. Additionally, the response of the neutron detectors to fast and slower neutrons can be tested with reactions that calibrate their energy response . In the first instance this may be done with cosmic muons [2] and Cf and AmBe sources that give $\sim$ 10 MeV neutrons.
From this test run it would be sensible to have a beam selection of every other pulse giving $\sim$ 160 ns between beam bursts.
Typical (^{3}He,n) L=0 differential cross-sections [3] peak at less than 1.0 mb/sr for the transition to ground states and usually not more than 1.0 mb/sr for excited states (Fig. 5). Hence the main challenge is going to pick out about 1 in 10^3 γ-rays in coincidence with fast neutrons. It will therefore be advantageous to have the digital electronics on AFRODITE to be able to run at better than twice the rate using the analogue electronics. If standard experiments on AFRODITE can collect $10^9\gamma\gamma$ coincidences using the digital electronics, it should be possible to obtain $10^5\gamma\gamma - n_f$ coincidences to the few 0^+ excited states in the nucleus. Most of these 0^+ states will decay through the lowest 2^+ level.

Typical (^{3}He,n) L=2 differential cross-section [3] peak at an angle of 15 degree to 20 degree (Fig. 5). These L=2 transfers can be selected by moving the neutron detectors away from the beam line to be centered around 17.5 degree.

As the high resolution will come from detection of γ-rays and there can be a large 20 % variation in the energies of the fast neutrons from the (^{3}He,n) reaction, it is possible to use very thick targets. The beam energy choice and target thickness choice only have to ensure that the beam reaching the beam stop is not above the Coulomb Barrier for Bi, 22.4 MeV. The collisions between

the ^{3}He projectiles on the bismuth nuclei from the beam stop are below the Coulomb Barrier Eb = Â 22.4 MeV. Hence the stopping of the ^{3}He projectiles is not expected to yield a large amount of gamma rays and the emission of neutrons is very unlikely

B.3.3 CHOICE OF TEST REACTIONS

We have been interested recently in the properties of excited 0^+ states in N=88 and 90 nuclei. We have shown that the first excited 0_2^+ state in even-even nuclei with these neutron numbers are neutron two-particle, two-hole states based on the high-K [505] $11/2^-$ Nilsson extracted be the deformation from lower shell. This state behaves like a (second vacuum) with reduced pairing due, in part to the low density of (oblate) states with negative quadruple moments. The usual methods of populating states do not favor low spins and populating 0^+ states is even more difficult due to their low (2J+1) statistical weight. Very beautiful work to find 0^+ states has been carried out at the University of Kentucky using the (n,n) reaction with mono-energetic neutron beams. The problem with this approach is that gramme quantities of separated isotopes are needed and studies are limited to stable nuclei.

The (p,t) and (t,p) reactions have been widely used (Fig. 1) for neutron configurations but there is a paucity of data on two proton configurations. We are interested to discover at what excitation energy the lowest two proton paired states exist in ^{154}Gd. Hence we would like to start our tests of the applicability of the method using the ^{152}Sm(^{3}He,n)^{154}Gd reaction at a beam energy of 22.5 MeV. We currently have the 4 mg cm^2 ^{152}Sm targets.

Four excited 0 states are known in 154 Gd (Fig. 1);

State	E_x(keV)	$E_{\gamma 1}(2_1^+)$(strength)	$E_{\gamma 2}(2_2^+)$	$E_{\gamma 3}(2_3^+)$
0_2^+	680.7	557.5		
0_3^+	1058.9	1058.9 (100)	366.5(18)	
0_4^+	1574.0	1451.2 (27)	758.5 (100)	577.7 (85)
0_5^+	16.50.3	1527.1 (100)	834.9 (17)	

If we expect 0^+ states at higher energies, in particular near the top of pairing gap at $E_x > 2$MeV, we will expect these to have strong, or at least significant, decays to the first excited 2^+ state at 123 keV. Hence we will need to detect γ-rays up to at least 4 MeV.

REFERENCES

[1] M. A. M. Shahabuddin et al., Nucl. Phys. A340 (1980) 109.
[2] Victor Makondelele Tshivhase, PhD thesis UCT 1997.
[3] W. P. Alford et al., Nucl. Phys. A321 (1997) 45.

Bibliography

[1] M. Shahabuddin *et al., Nucl. Phys. A 340, 109 (1980).*

[2] R.T. Newman *et al. Proceeding of Balkan School on Nucl. Phys*, Balkan Phys. Lett. 182 (1998).

[3] M. Dasgupta *et al., Annu. Rev. Nucl. Part. Sci. 48, 427 (1998).*

[4] National Nuclear Data Center web site. *Chart of Nuclides, A list of levels and a level scheme (2011).*

[5] T. Baumann. *National Superconducting Cyclotron Laboratory Michigan State University*, 4 (2001).

[6] N. S. Bowden *et al., ArXiv: 0908.1206V1. [pysics.ins-det] (2009).*

[7] J. R. D Copley *et al., Journal of Research of the National Institute of Standards and Technology. 98 N, 1 (1993).*

[8] B. Povh *et al., Particles and nuclei: an introduction to the physical concepts, Springer. Springer (2008).*

[9] N. Mascarenhas *et al., IEEE Xplore. 53 Issue: 4, 2233 - 2237 (2006).*

[10] B. Luther *et al., Nucl. Instr. And Methods. A 505, 33 (2003).*

[11] S. Prestemon *et al., IEEE Trans. Appl. Supercond. 11, 1721 (2001).*

[12] S. Prestemon *et al., IEEE Transactions on Nuclear Science. 15, 1252 (2005).*

[13] D. Bazin *et al., Nucl. Instr. and Meth. B 204, 629 (2003).*

[14] N. Aoi *et al., Phys. Rev. C, vol. 66, p. 014301 (2002).*

[15] G. Perdikakis *et al., Proceedings of the Symposium on Radiation Measurements and Applications (SORMA West 2008), Berkeley, California, June 2-5, 2008 . IEEE Trans. Nucl. Sci. 56, 1174 (2009).*

[16] G. K. Mabala. PhD thesis, University of Cape Town.

[17] G. F. Knoll. *Radiation Detection and Measurement.* John Wiley Sons (1989).

[18] V. Bom. *SM/EN-20*, Mekelweg 15, 2629 JB Delft, the Netherlands (2010).

[19] S. Taniguchi *et al., Elsevier Science. SLAC-Pub-9506, 1 (2002).*

[20] T. Gooding and H. Pugh. *Nucl Instrum Meth*, 7, 189-192 (1960).

[21] V. M. Tshivhase. PhD thesis, University of Cape Town (1997).

[22] K. Y. Nam *et al., IEEE Xplore.* 0-7803 (1999).

[23] http://www.xia.com.

[24] Mark Pearce. *Section of Experimental Particle Physics, KTH*, version 3 (2003).

[25] M. Lipoglavsek *et al., Nucl Instrum Meth.* (2005).

[26] Maxim Integrated Products. volume Analog to Digital Converter (2000).

[27] W. L. Bryan *et al., Oak Ridge National Laboratory, USA.* (2003).

[28] M. Tanaka *et al., IEEE Transaction on Nuclear Science.* KEk Preprint 92-114 (1992).

[29] K. Carnes. *Introductory Nuclear Physics.* John Wiley Sons (1987).

[30] E. Kowalski. *Nucl Instrum Meth, North-Holland Publishing CO*, 52, 357 (1967).

[31] P. Papka *et al., Phys. Rev. C.* 75, 045803, 31 (2007).

[32] R. Brun and F. Rademakers. *http://root.cern.ch/*, A 389, 86 (1997).

[33] P. Söderström. *ArXiv: 0804.2417V1 [nucl-ex] (2008).*

[34] S. S. Ntshangase *et al., Phys. Rev. C. 82, 041305 (R) (2010).*

[35] D. Mahboub *et al.,* Phys. Rev. C. *16 034616 (2004).*